Journal of African Earth Sciences 233 (2026) 105891

Contents lists available at ScienceDirect

Journal of African Earth Sciences

journal homepage: www.elsevier.com/locate/jafrearsci

Subsurface magmatic structure beneath the nested Awasa-Corbetti caldera complex, Main Ethiopian Rift, as determined from gravity data

Simeneh Wassihun [a,b], Abera Alemu [a], Wubamlak Nigussie [c,d], Kevin Mickus [e,*], Derek Keir [f,g], Shimels Wendwesen [h], Habtamu Wuletawu [i]

[a] School of Earth Sciences, Addis Ababa University, Addis Ababa, Ethiopia
[b] Department of Geology, Mekdela Amba University, Tulu Awulia, Ethiopia
[c] Department of Earth Sciences, Memorial University of Newfoundland, St. John's, NL, Canada
[d] School of Earth Sciences, Bahir Dar University, Bahir Dar, Ethiopia
[e] Department of Geosciences, Missouri State University, Springfield, United States
[f] School of Ocean and Earth Science, University of Southampton, Southampton, United Kingdom
[g] Dipartimento di Scienze Della Terra, Università Degli Studi di Firenze, Florence, Italy
[h] Department of Geology, Dire Dawa University, Dire Dawa, Ethiopia
[i] Department of Water Resource and Irrigation Engineering, Wallaga University, Nekemte, Ethiopia

ARTICLE INFO

Handling Editor: M Mapeo

Keywords:
Awasa-corbetti caldera complex
Magma plumbing systems
Mafic intrusions
2D gravity modeling
Main ethiopian rift

ABSTRACT

The nested Awasa–Corbetti caldera complex (ACC) in the central Main Ethiopian Rift (MER) encompasses the Corbetti caldera complex, which is presently one of the volcanoes undergoing the most rapid uplift in the region and with notable seismic activity. Previous studies provided limited insight into the subsurface crustal structure and the magma plumbing systems beneath this active volcano. To address this gap, we used terrestrial gravity data combined with geological mapping, seismic, and magnetotelluric models to image the crustal structure. We analyzed the gravity data using wavelength filtering, upward continuation, and 2D forward modeling. Gravity anomaly maps show magmatic intrusions beneath the Corbetti and Shalla caldera complexes and the eastern rift margin (Wondo Genet volcanic zone). 2D density models indicated that these intrusions lie at depths of approximately 10–20 km beneath Corbetti, 7–12 km beneath Shalla, and 5–7 km beneath the Wondo Genet volcanic zone. Upward continuation and band pass filtering suggest that the individual caldera complexes have discrete intrusions within the upper crust, with a larger magmatic intrusion that is continuous beneath all of the caldera complexes in the mid to lower crustal depths. The upward continuation and band-pass gravity anomaly maps also reveal volcanic zones along the rift borders (Wagebeta and Chike), indicating that dike injection has added magma along the rift margins. On a regional scale, the gravity maxima align with WNW-ESE-trending intra-rift structures that crosscut the MER. These anomalies show spatial correspondence with the Goba-Bonga volcano-tectonic lineament, suggesting that this inherited structural discontinuity may facilitate magma transport both in the rift margin and in the nested ACC. By integrating 2D gravity, geological, geodetic, seismic, and magnetotelluric models, we created a 3D conceptual model. This model reveals that a network of deep mafic intrusions and shallow mafic intrusions supplies the upper crust beneath the Corbetti and Shalla caldera complex, correspondingly. Our results show that rift evolution in the middle and latter stages occurs from dike intrusion but may also include magmatic processes that occur just outside the rift.

1. Introduction

The Main Ethiopian Rift (MER) (Fig. 1) is a continental, magma-rich rift that connects the Kenya Rift to the south and the Afar Rift to the north (Hayward and Ebinger, 1996; Casey et al., 2006). During the Quaternary, the focus of extension changed from fault-dominated to magma-assisted rifting, especially in the northern sections of the MER (Rooney et al., 2011). The MER initially formed in the Miocene with crustal extension mainly concentrated along the border faults (Wolfenden et al., 2004; Corti, 2009). During the Quaternary, however,

* Corresponding author.
E-mail address: kevinmickus@missouristate.edu (K. Mickus).

https://doi.org/10.1016/j.jafrearsci.2025.105891
Received 18 December 2024; Received in revised form 29 September 2025; Accepted 14 October 2025
Available online 15 October 2025

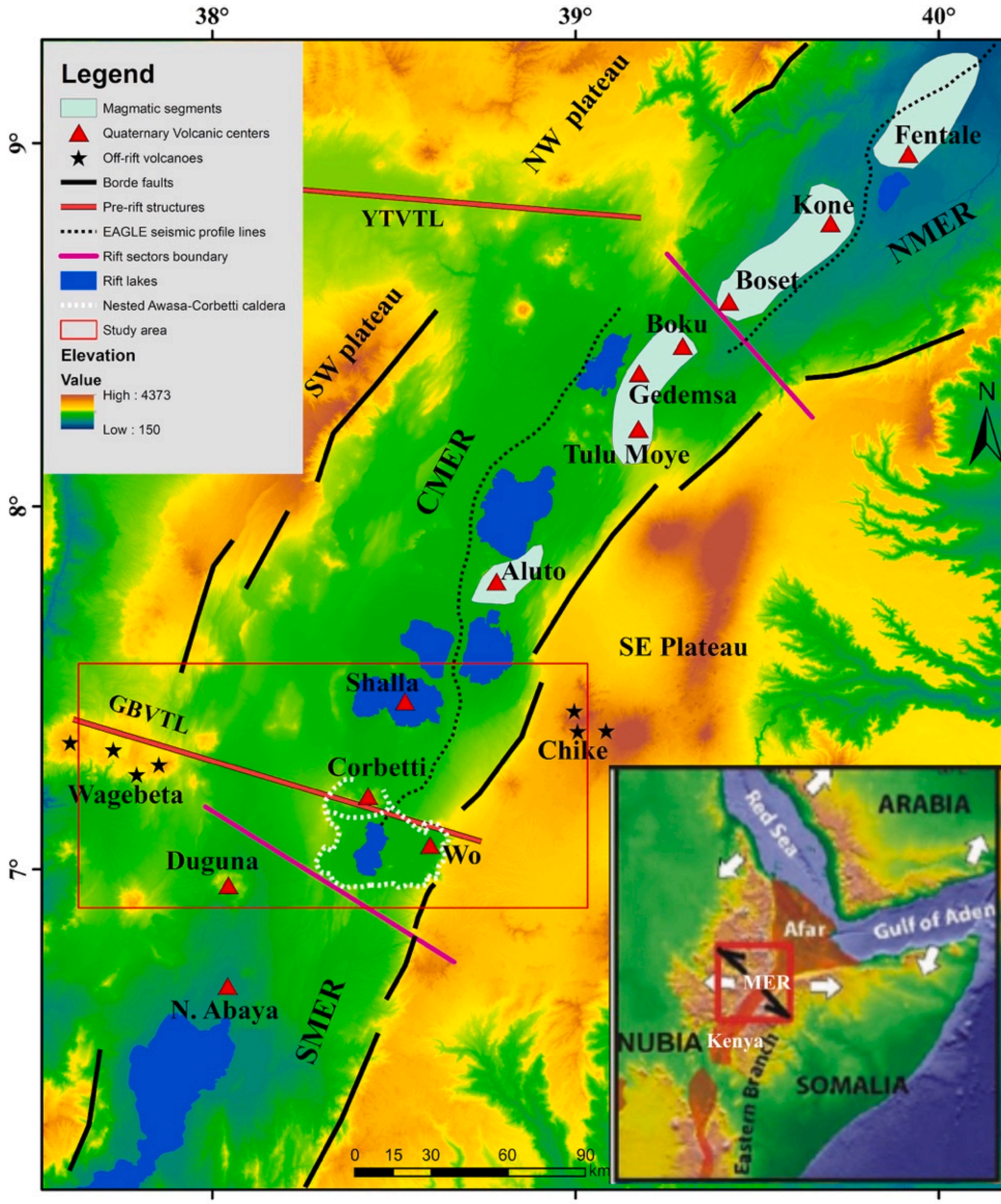

Fig. 1. Digital elevation map of the central Main Ethiopian Rift (CMER) showing the location of the border faults (black lines), major volcanic centers (red triangles), and major structural trends (red lines). The study area is shown by a red box. The different rift segments are separated by pink lines. Wo-Wondo Genet volcanic zone, YTVTL-Yerer-Tulu volcano tectonic lineament, GBVTL-Goba-Bonga volcano tectonic lineament, NMER-northern Main Ethiopian Rift, SMER-southern Main Ethiopian Rift. Inset map shows the location of the study area (red box) within Ethiopia and the surrounding area. Nubia, Somalia, and Arabia are different tectonic plates. Brown areas represent the East African Rift. White and black arrows show the relative movements of the plate and the rift (Boccaletti et al., 1998; Wolfenden et al., 2004; Rooney et al., 2011). DEM source (https://search.asf.alaska.edu/#/?dataset=ALOS). (For interpretation of the references to color in this figure legend, the reader is referred to the Web version of this article.)

extension became more localized due to dike intrusion on the rift floor within en-echelon, narrow (~20 km wide) magmatic segments that contain Quaternary to Recent volcanic centers (stratovolcanoes and calderas), and sometimes aligned volcanic cones (Fig. 1) (Ebinger and Casey, 2001; Peccerillo et al., 2003; Corti, 2009; Siegburg et al., 2020) in the northern MER (NMER) and portions of the central MER (CMER). This thermo-mechanical weakening promotes localized deformation, crustal thinning, and may ultimately lead to the transition from continental rifting to oceanic spreading, a process observed in mature rift systems like the Red Sea (Buck, 2006). As a result, the MER is an ideal place to understand how magma plumbing systems develop and modify crustal structure during rifting.

Geodetic and geophysical observations within the last two decades have identified several actively deforming caldera complexes within the CMER, specifically at Corbetti, Aluto, Tulu Moye, and Boku (Fig. 1) (Biggs et al., 2009; Hutchison et al., 2016a, 2016b, 2018; Lloyd et al., 2018; Lavayssière et al., 2019; Gottsmann et al., 2020; Wuletawu et al., 2024, 2025). The Corbetti caldera complex is among the most rapidly deforming volcanoes globally, exhibiting an uplift rate of approximately 7 cm/yr (Lloyd et al., 2018). This substantial deformation is correlated with persistent micro-seismicity (Lavayssière et al., 2019), suggesting active magma migration or pressurization beneath the edifice. The Corbetti caldera complex is located within the nested Awasa-Corbetti Caldera Complex (ACC) (see the white dotted polygon in Fig. 1), where extensional processes occur along both the border faults and the magmatic segments (Fig. 1; Woldegabriel et al., 1990; Corti, 2009; 2018). These characteristics render it an optimal site for investigating the development and dynamics of magma plumbing systems during continental rifting. Although its surface geology (Woldegabriel et al., 1990; Colby et al., 2022), structural setting (Maestrelli et al., 2021; Corti et al., 2018), geochemical and isotopic signatures (Hutchison et al., 2016a, 2016b, 2018), and deformation activity (Gottsmann et al., 2020) are relatively well-characterized, the nature of the subsurface magmatic structure and the associated plumbing systems feeding the caldera complexes remain unclear.

Recent geophysical investigations, including magnetotelluric (MT) studies (Dambly et al., 2024) and microseismicity analyses (Lavayssière et al., 2019), have advanced our knowledge of the distribution of magmatic-hydrothermal fluid zones within the crust beneath the Corbetti caldera complex. Although these subsurface analyses only investigate the Corbetti caldera complex, we lack a comprehensive understanding of the subsurface characteristics of the larger ACC. Moreover, despite the region being marked by recent/Holocene caldera collapses and shaped by both along-rift floor faults (Fig. 2a and b) and cross-rift pre-existing structures (Goba-Bonga volcano-tectonic lineament (GBVTL) (Fig. 1; Corti et al., 2018), the subsurface connections

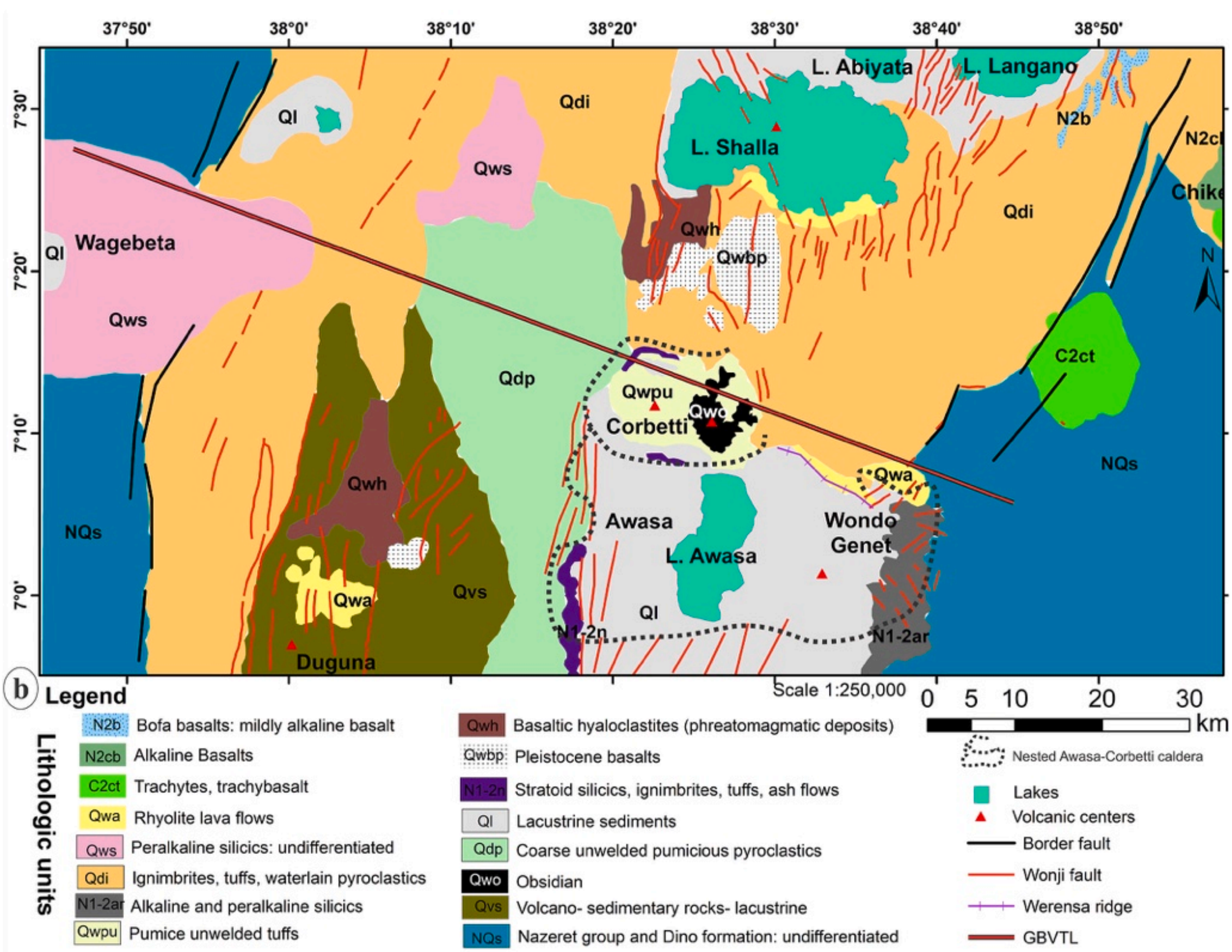

Fig. 2. Geological and tectonic setting of the study area. (a) Geological and structural map of the region (EIGS, 2012). (b) Hillshade map illustrating the tectonic and structural framework of the nested Awasa–Corbetti caldera complex. Wk-Wondo Koshe volcanic edifice. GBVTL-Goba-Bonga volcano tectonic lineament. DEM source is similar to Fig. 1.

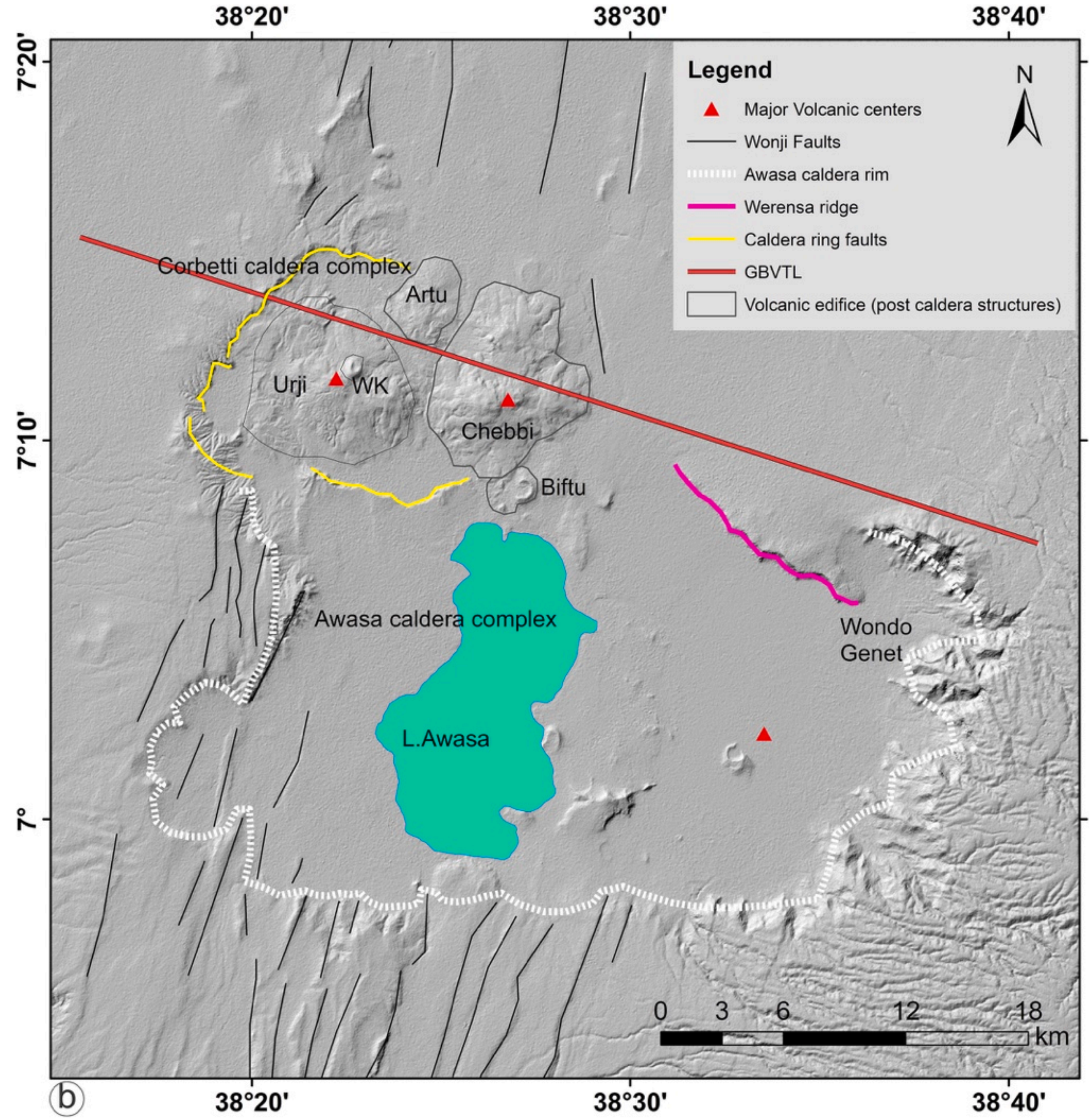

Fig. 2. (*continued*).

between volcanic systems and fault networks, as well as the overall subsurface architecture of the magma plumbing systems beneath the ACC, are not well-defined.

We used terrestrial gravity data to image the magma plumbing systems beneath the nested ACC and surrounding regions. Gravity data can provide constraints on the nature (location, depth, and density) of the magmatic systems that complement the models determined by seismic and MT data in the MER. Unlike the seismic (specifically shear waves) and MT methods which are better suited than gravity to image potential melt and fluid rich regions, gravity is better at imaging solidified intrusions which commonly does not produce notable seismic or electrical resistivity anomalies (Mickus et al., 2007) and may be able to distinguish between shallow dikes (high-frequency anomalies) from deeper mush zones (low-frequency anomalies). While MT struggles to differentiate crystal-rich mush from solid intrusions, and seismic faces challenges with shallow melt (Keranen et al., 2004), a gravity analysis bridges these gaps. Our study integrates gravity data with existing MT and seismic models to reduce the non-uniqueness of each method (e.g., discriminating melt vs. solidified intrusions). No single geophysical method is superior to another, but a combined approach has the potential to yield the most plausible results. We present a series of gravity anomaly maps, two-dimensional (2D) forward models, and three-dimensional (3D) conceptual models supported by the existing geological (Corti et al., 2018; Colby et al., 2022; c), geodetic (Lloyd et al., 2018), geochemical and isotopic (Hutchison et al., 2016b; 2018), and geophysical data (Maguire et al., 2006; Mickus et al., 2007; Gíslason et al., 2015; Lavayssière et al., 2019; Gottsmann et al., 2020). Our comprehensive analysis aims to enhance the understanding of the subsurface magma plumbing systems, the tectono-magmatic interlinkage (structural and magmatic connections between pre-existing tectonic features (like the GBVTL), active fault systems (rift axis faults), and magmatic intrusions), and the deep heat source beneath the nested caldera and its environs. For the ACC and the surrounding region, we provide the first caldera-scale resolution of the intrusions as prior rift-wide gravity studies (Tiberi et al., 2005; Mickus et al., 2007, 2009) lacked the spatial density to resolve individual caldera systems, whereas our high-pass filtering (<20 km wavelengths) maps the subsurface structures beneath the Wondo Genet volcanic zone and Shalla caldera complex, revealing previously unrecognized shallow intrusions. These findings have implications for the other active volcanoes in the MER and the broader East African Rift System.

2. Geologic setting and prior geophysical work

2.1. Geology and tectonic setting

The MER is the northern segment of the East African Rift System, connecting the Kenya Rift with the Afar Triple junction (Wolfenden et al., 2004). The MER contains two predominant normal fault systems: the Miocene border faults and the Quaternary-Recent rift floor faults. Collectively, these systems are known as the Wonji Fault Belt (WFB) (Fig. 2a and b; Boccaletti et al., 1998; Bonini et al., 2005). Cross-rift volcano-tectonic zones such as the GBVTL and the Yerer-Tulu volcano-tectonic lineament (YTVTL) are also prominent features. Rift initiation varied 5–21 Ma, where the southern MER (SMER) and the NMER segments were initiated at 21 Ma and 11 Ma, respectively. These sections were subsequently unified by the opening of the CMER at 5 Ma, which underwent substantial extensional deformation (Woldegabriel et al., 1990; Wolfenden et al., 2004; Bonini et al., 2005). The MER is characterized by a complex interlinkage of the border and rift floor faults, cross-rift features (GBVTL), and several nested calderas (refers to a complex of two or more collapse structures where a younger caldera has formed partially or entirely within the boundary of an older one, the common example is the ACC) and caldera collapse features (fault, fracture, and depression with single collapse event) (Woldegabriel et al., 1990, Figs. 1 and 2a). While the nested ACC is associated with transverse WNW-ESE trending structures (GBVTL) and NNE-SSW rift floor faults (WFB) (Fig. 2a and b; Acocella et al., 2002), the detailed subsurface interlinkage of these structures is scarce. Surface-based geological and structural studies report an overlap between the marginal faults of the eastern rift and the eastern wall of the Awasa caldera (EIGS, 2012, Fig. 2; Di Paola, 1971; Woldegabriel et al., 1990). Lloyd et al. (2018) proposed a subsurface interlinkage between the Werensa ridge and the eastern rift margin (Wondo Genet Volcanic zone) with the GBVTL, intersecting the rift boundary (Fig. 2a and b), based on a combined analysis of interferometric synthetic aperture radar, global positioning system data, and a network of seismometers. However, while such methods are powerful in detecting active deformation, they have limited resolution in imaging the interaction of subsurface structures with magmatic bodies and/or hydrothermal fluids. As a result, further work is needed using appropriate methods (see section 2.3 and section 3) to outline the precise subsurface extent and interaction of nested caldera features with rift-related faults and cross-rift structures.

2.2. Collapse calderas within the CMER

The analysis of caldera formation within the CMER is complicated by rapid caldera collapse and subsequent burial by any recent volcanic activity and sediments (Maestrelli et al., 2021). As a result, identifications of caldera features in the region need detailed surface and subsurface studies. However, several collapse calderas such as Gedemsa, Aluto, Shalla, and Corbetti have already been identified mainly from a surface geological study (Acocella et al., 2002). The Corbetti caldera complex overlaps the larger Awasa caldera complex, forming a nested caldera system likely resulting from a multi-phase collapse (Fig. 2b; Di Paola, 1971, 1972; Rapprich et al., 2016; Maestrelli et al., 2021; Colby et al., 2022). However, whether the deep magmatic source for the two-caldera complexes is the same or not remains unclear. The Corbetti caldera complex is dissected by WNW-ESE-oriented faults (Fig. 2b), which were reactivated pre-existing crustal weaknesses (Lloyd et al., 2018; Hunt et al., 2019). The volcanic history of the Corbetti caldera complex is associated with shield volcano development and the eruption of pyroclastic deposits, with three post-caldera structures (Artu, Urji, Chabbi) and two recent cones (<10 ka) (Wendo Koshe pumice and Biftu tuff) (Rapprich et al., 2016; Colby et al., 2022). Hutchison et al. (2018) showed that the caldera complexes within the MER have been associated with frequent earthquakes, ground deformation, and the release of gases. However, a complete understanding of the region needs integrating surface-based mapping studies with subsurface imaging methods, such as potential field, also called structural geophysical methods (section 2.3 and section 3), are needed to outline the interlinkage between rift-related faults, collapse calderas, and intrusions, and to reconstruct the overall tectonic-volcanic development of the nested caldera complexes in the region.

2.3. Previous geophysical framework

The regional crustal and lithospheric mantle framework of the MER was deciphered by the Ethiopia Afar Geoscientific Lithospheric Experiment (EAGLE), which created wide-angle reflection/refraction models (Fig. 3; Mackenzie et al., 2005; Maguire et al., 2006). These models indicated a crustal thickness of ~35 km beneath the rift and ~40 km beneath the Southeast Plateau. In contrast, the crust beneath the Northwest Plateau is approximately 45 km thick and features high-velocity lower crustal regions, interpreted as mafic underplating (Mackenzie et al., 2005; Kibret et al., 2022a). Passive seismic modeling, including teleseismic receiver functions, in general agrees with the crustal depths determined by wide-angle seismic studies (Hammond et al., 2011; Kibret et al., 2022b). The seismic receiver functions also helped constrain the compressional and shear wave velocity ratios (Vp/Vs) and revealed that the crust beneath the rift valley has high values > 1.9 to 2.0 (Stuart et al., 2005; Hammond et al., 2011), which was further supported by surface-wave modeling (Chambers et al., 2019, 2022). Regions with elevated Vp/Vs ratios are attributed to continental crust modified by mafic intrusions (Chambers et al., 2021), which is also supported by regional gravity modeling (Mahatsente et al., 1999; Tiberi et al., 2005; Mickus et al., 2007; Mammo, 2013; Nigussie et al., 2023a). Gravity modelling of the MER (Mickus et al., 2007) revealed a gravity maximum occurring over the magmatic segments, caused by mafic intrusions into the lower and upper crust (7–10 km) (Fig. 3b). Additionally, Nigussie et al., 2023b used the Global Gravity model plus (GGMplus, 2013) to map the subsurface structure of magmatic segments in the central and northern MER transition. Their results suggest that magmatic segments have discrete subvolcanic plumbing systems, at least down to mid-crust levels, with magma injection accommodating extension at the segment centers and faulting dominating towards the segment ends. Similar gravity modelling (Nigussie et al., 2023b; Wendwesen et al., 2025) shows the absence of linkage between Aluto and Gedemsa magmatic segments, and both studies proposed that the former is linked to and controlled by transversal structures in the rift, whereas the latter is controlled by dyke intrusion. This observation challenges surface structural mapping (Ebinger and Casey, 2001; Kurz et al., 2007), which argues that Aluto and Gedemsa volcanoes belong to a single magmatic segment. Conversely, 2D gravity modeling over Gedemsa and Boku volcanic centers (Nigussie et al., 2022; Wuletawu et al., 2024) reveals discrete and shallow magma plumbing systems

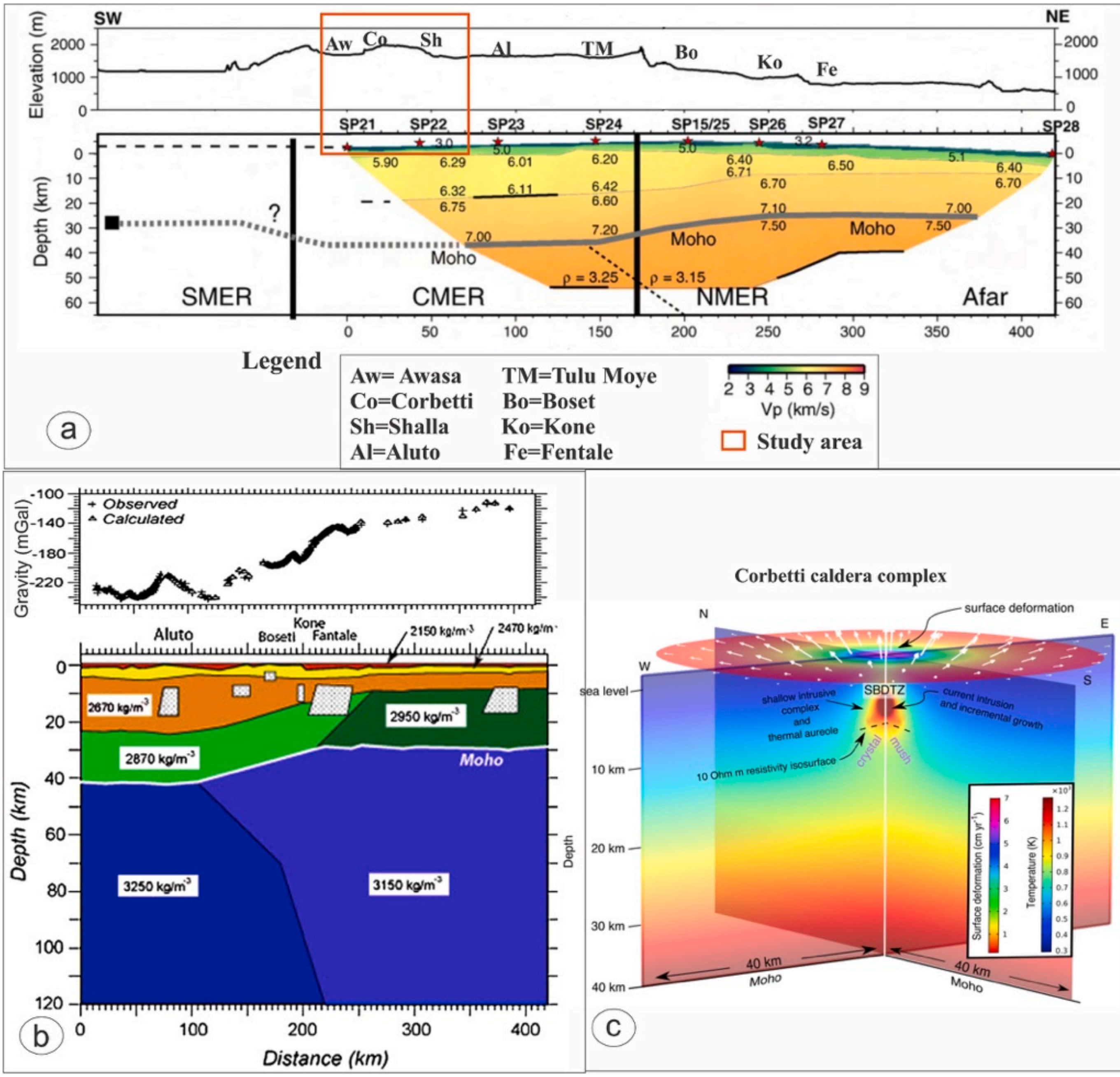

Fig. 3. We used previous geophysical work as a reference for our models. (a) Two-dimensional seismic refraction models from the Ethiopian-Afar Geoscientific lithospheric experiment (EAGLE) along the MER axis (modified from Maguire et al., 2006) were used as an initial model for the 2D forward gravity models (Fig. 9a–c). The vertical black solid lines represent the boundary between the southern Main Ethiopian Rift (SMER), central Main Ethiopian Rift (CMER), and northern Main Ethiopian Rift (NMER). The solid gray line is the depth to the Moho, and the dashed gray line is the approximate depth to the Moho. The black dashed line illustrates the contrast in upper mantle density between the CMER (3.25 kg/m^3) and the NMER (3.15 kg/m^3) (Mickus et al., 2007). (b) Two-dimensional gravity model along the main axis of the MER. Bodies with a white fill pattern are mafic with a density of 3.00 g/cm^3. (c) Schematic illustration of the upper-crustal plumbing system beneath Corbetti caldera complex, integrating geodetic and gravimetric surveys with data modeling (Gottsmann et al., 2020). Key features include the seismically defined brittle-ductile transition zone (SBDTZ) (Lavayssière et al., 2019; Dambly et al., 2024) at ~7 km depth and the deep conductive zone (10 Ωm isosurface; Gíslason et al., 2015), as inferred from geophysical observations.

sourced from a single deeper magmatic intrusion zone, suggesting the same magmatic segment for the two volcanic centers. However, these studies highlight the importance of subsurface mapping methodologies; they are limited to the central to northern MER, other magmatic segment zones, and collapse calderas-further south, such as the nested ACC system, the target of these studies, is poorly understood.

According to Lavayssière et al. (2019), the Corbetti caldera complex is currently experiencing significant seismic and magmatic activity, although the underlying cause remains uncertain. InSAR data indicated an uplift rate of 7 cm/y at the Corbetti caldera complex (Lloyd et al., 2018). Additionally, joint geodetic and microgravity modeling (Fig. 3c; Gottsmann et al., 2020) indicated dense, mafic magma intrusions at approximately 7 km depth beneath the Corbetti caldera complex. These findings, along with magma intrusion models derived from MT studies (Dambly et al., 2024), suggest that the observed uplift is more closely related to magmatic processes rather than hydrothermal activity (Gottsmann et al., 2020). MT studies also indicate the migration of hydrothermal fluids at shallower depths (Gíslason et al., 2015).

Previous research has primarily focused on the Corbetti caldera complex, leaving the upper crustal anatomy of the surrounding regions, including Shalla, Wondo Genet, and off-rift volcanoes, largely unexplored. Pre-rift structures, such as the GBVTL, may play a role in facilitating magma transport and influencing shallow hydrothermal processes (Lloyd et al., 2018; Dambly et al., 2024). These rift structures also align with the observed spatial patterns of seismicity (Keir et al., 2009). Liu et al. (2019) document analogous magma-assisted rift dynamics in other magmatic rifts, such as the Rio Grande Rift, where pre-existing structures control melt ascent. Recent studies in the Auckland volcanic field in New Zealand demonstrate that pre-existing crustal structures significantly influence magma ascent pathways, as revealed by gravity modeling (Luthfian et al., 2023).

3. Data and methodology

3.1. Gravity dataset

This study utilizes terrestrial gravity data obtained from the National Geospatial and Imaging Agency (https://www.nga.mil/). We analyzed a total of 3720 gravity data points, with station intervals ranging from 5 to 0.1 km (Fig. 5). The data distribution is good enough within the nested ACC to be able to characterize the subsurface magmatic structures at both local and semi-regional scales.

3.2. Methods

3.2.1. Gravity data processing

The terrestrial gravity data represent the measured gravity values. We calculated the theoretical gravity values for each reading by using the Geodetic Reference System 1967 (GRS67). We processed the entire gravity dataset into complete Bouguer gravity anomalies (CBA) by applying corrections for latitude, elevation, and topography. We used sea level as a datum and a density reduction of 2670 kg/m^3. Terrain corrections were calculated using a 12.5 m digital elevation model (DEM) and an average crustal density of 2670 kg/m^3. To generate the CBA map (Fig. 4), the data were gridded or regularly interpolated onto square grids of 0.25 × 0.25 km using the minimum curvature method in Geosoft Oasis Montaj version 8.4 software. We also used the module MAGMAP1 GX of Oasis Montag to do a one-step grid filtering by applying common Fourier domain filters to the gridded gravity data.

3.2.2. Anomaly separation and data enhancement

The CBA map contains the aggregate effect of long and short wavelength anomalies caused by shallow and deeper density sources. To analyze the upper crustal density sources, we enhanced the CBA data using upward continuation, frequency filtering, and polynomial surface fitting to emphasize the relevant anomalies (e.g., Mickus et al., 1992). We applied a low-pass Gaussian filter to the CBA data, removing wavelengths greater than 80 km to produce a regional gravity anomaly map (Fig. 5). As a general guideline, the depth to the source of the causative density is roughly one-quarter of the wavelength (Abera,

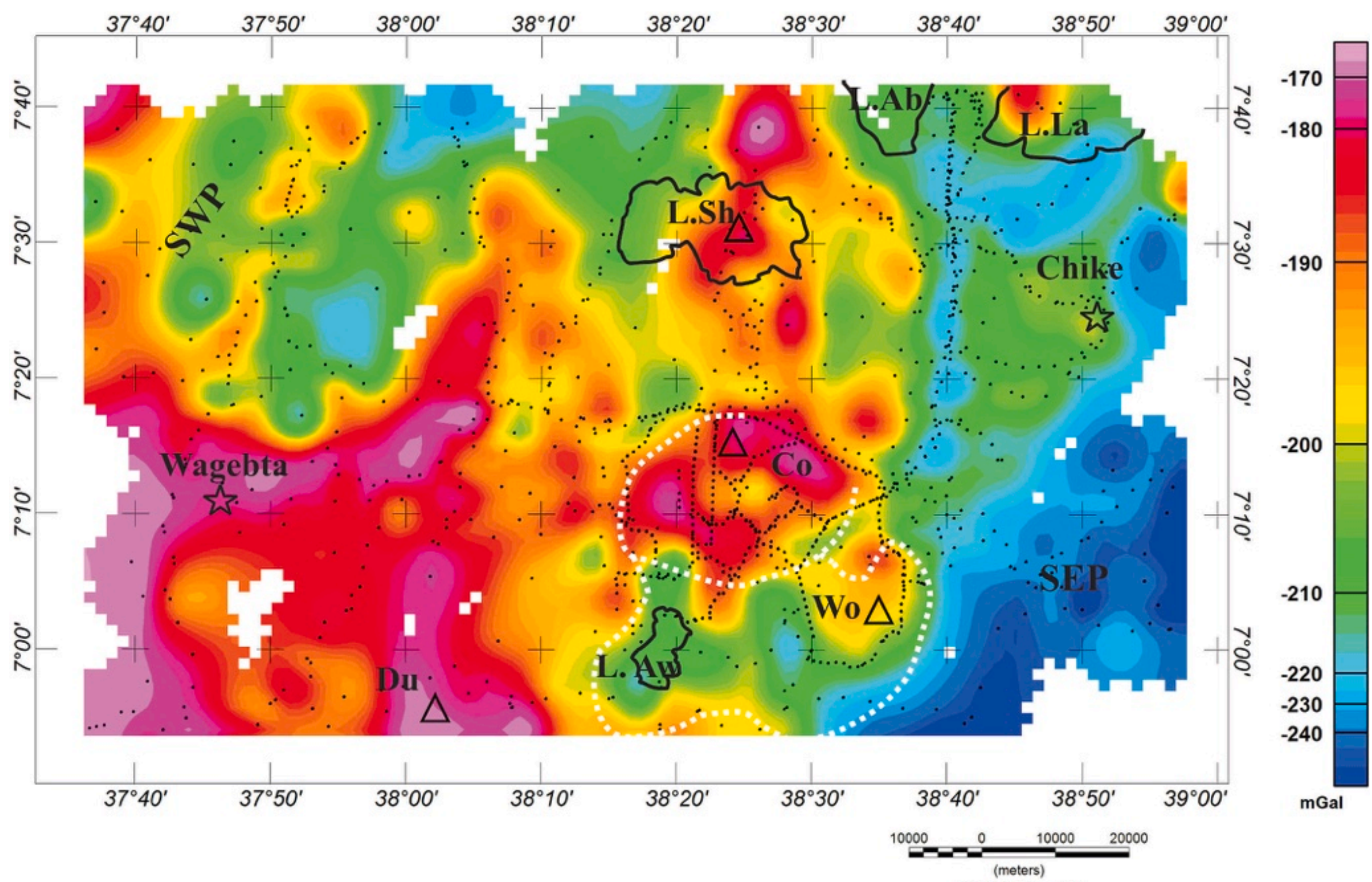

Fig. 4. Complete Bouguer gravity anomaly map of the nested ACC and the surrounding region, where the black dots are the location of the gravity stations. Lake Awasa-L.Aw, Lake Shalla-L.Sh, Lake Abiyata-L.Ab, Lake Langano-L.La, Corbetti caldera complex-Co, Duguna magmatic zone-Du, Wondo Genet volcanic zone-Wo, Southwest Plateau-SWP, Southeast Plateau-SEP. The white dotted polygon represents the boundary of the nested ACC. The black lines represent rift floor lakes. The triangular shape symbols represent volcanic centers (Corbetti, Wondo Genet, Shalla, and Duguna), and the black stars are off-rift volcanic zones (Wagebeta and Chike).

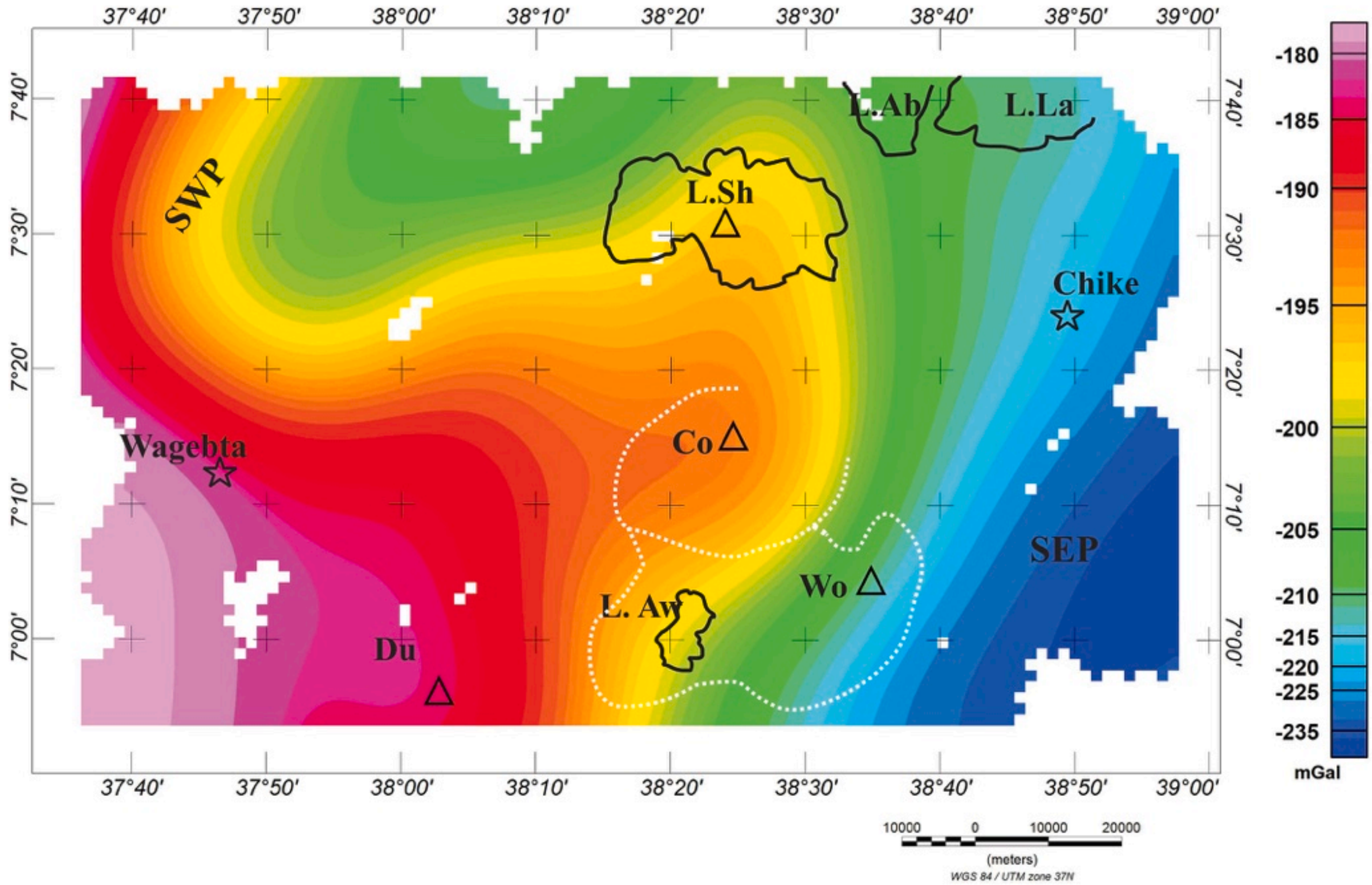

Fig. 5. Regional gravity anomaly map of the nested ACC and the surrounding region. Numbers 1–8 are anomalies discussed in the text. Abbreviations and symbols are the same as in Fig. 4.

2020). We created the residual gravity field (Fig. 6) by subtracting the regional gravity field from the CBA data (Fig. 4). Thus, the 80 km residual gravity model map enhances density sources at depths <20 km, which is the average depth of the upper crust in the MER (Mackenzie et al., 2005; Maguire et al., 2006).

We applied data enhancement methods, namely upward continuation and band-pass filtering, to estimate the depths of causative anomaly sources. Upward continuation height is a method that determines the gravitational field at various heights above the surface of the earth and thus, the continued gravity field becomes smoother and in general, represents deeper or broader density sources (Jacobsen, 1987). Upward continuation (heights from 5 to 30 km) were applied to determine the depth of various density sources (Fig. 7) while a 15–120 km band-pass filter was used to determine middle crustal density sources (Fig. 8). These mathematically based enhancement methods are good for approximate estimations of the depth to the density sources but these Fourier transform methods can create spurious anomalies that are not generally useable for quantitative data analysis (Hinze et al., 2013).

3.2.3. *Gravity forward modeling*

Linking subsurface structures to surface eruptive deposits, such as those at the nested ACC, remains challenging. While surface-based geological studies provide partial insights, geophysical methods such as gravity modeling offer a method to reveal the nature of the plumbing system of a volcano (Magee et al., 2018; Luthfian et al., 2023). Gravity modeling is inherently non-unique, where various subsurface density bodies can yield the same modeling result (Saltus and Blakely, 2011). The crustal structure of the MER, including the nested ACC and other similar volcanic areas, contains geological complex areas, where there are interactions between heat sources, fluid flow, and faults producing considerable density variability (Benti et al., 2023). Therefore, imaging the subsurface structures in these regions is particularly challenging due to the disparate responses of different data types to identical subsurface features. However, when constrained with seismic and MT models and geological data, gravity modeling can be a useful technique to understand lithosphere structure (Mickus et al., 2007). To address this ambiguity, multiple constraints were used, including seismic models (Maguire et al., 2006), MT models (Dambly et al., 2024), geological mapping (Di Paola, 1971; Woldegabriel et al., 1990), and stratigraphic data (Colby et al., 2022) to constrain the final gravity models. Nonetheless, the inherent difficulties in delineating subsurface characteristics, our integrative modeling represents one optimal option of the several geological scenarios that could explain the nested ACC and the surrounding regions.

We performed the 2D forward modeling using GM-SYS software from the Oasis-Montaji extension. The various density bodies were iteratively changed (horizontal and vertical locations, density values) to improve the fit between observed and calculated gravity anomalies. We constructed several models and selected the final ones based on their agreement with the external constraints. As a result, we constructed three profiles to model the upper crustal structures to depths of 20 km using the residual gravity field (Fig. 5). Data constraints (surface and subsurface rock formations and depths to various subsurface structures) were obtained from geological (Colby et al., 2022; Corti et al., 2018) and geophysical (Lloyd et al., 2018; Lavayssière et al., 2019) studies conducted within the nested ACC and its environs. We derived regional crustal structure from velocity models of the EAGLE seismic refraction studies (Fig. 3) (Maguire et al., 2006). We used the P-wave velocities from the EAGLE models to estimate the densities of the upper crustal bodies, applying the seismic velocity-density relationship from

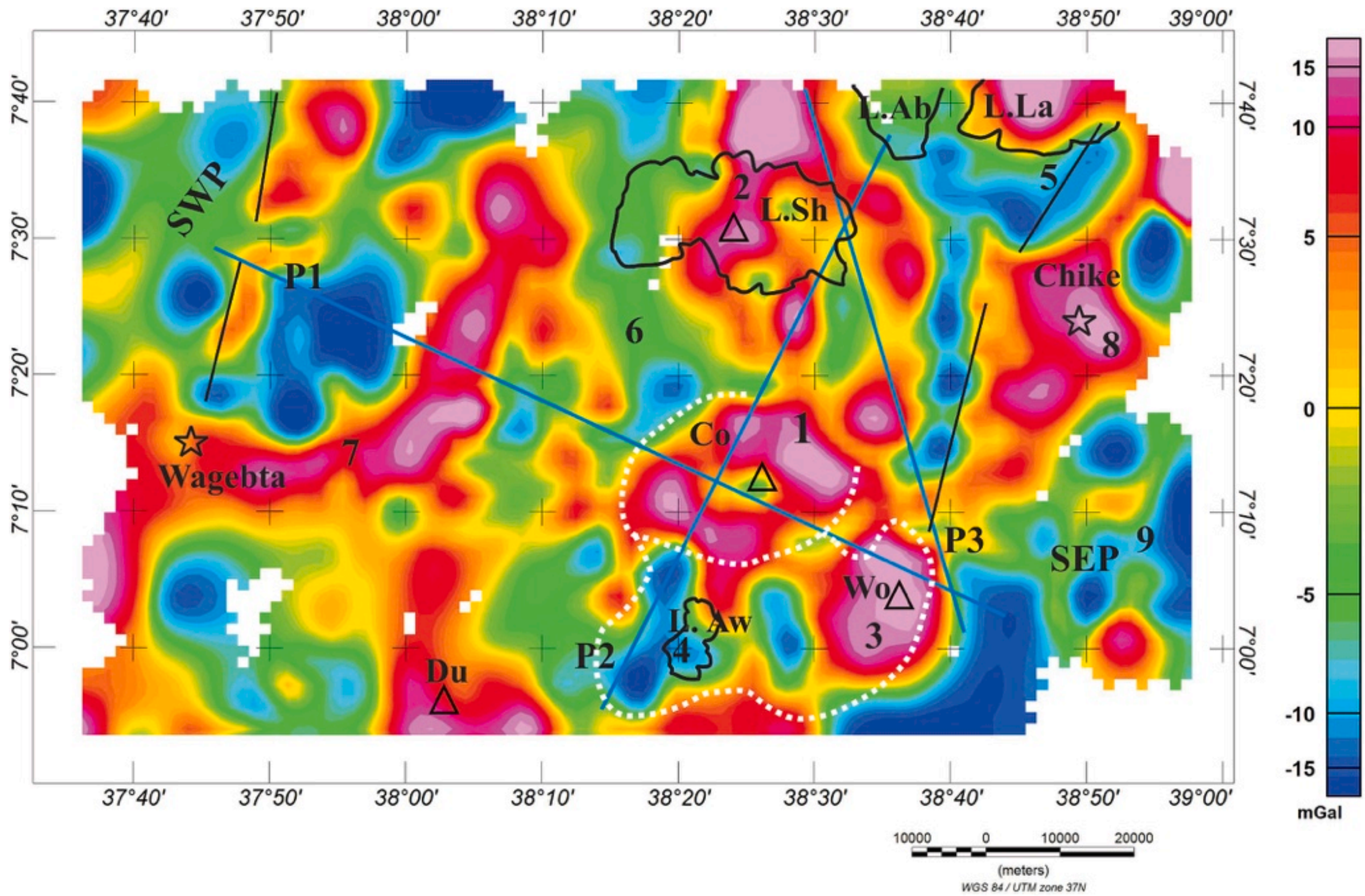

Fig. 6. Residual gravity anomaly map of the nested ACC and the surrounding region. The pale blue color lines P1, P2, and P3 are the locations of the gravity models. The black solid lines are rift border faults. Numbers 1–8 are anomalies discussed in the text. Abbreviations and symbols are the same as in Fig. 4. (For interpretation of the references to color in this figure legend, the reader is referred to the Web version of this article.)

Christensen and Mooney (1995). We converted the fastest and the slowest P-wave velocities in each layer to initial densities (Table 1) using:

$$\rho = -168.03 + 1765\, v\rho - 481.72 v\rho^2 + 60.973 v\rho^3 - 2.6861 v\rho^4$$

where ρ is the density of the subsurface in kg/m^3. Whereas $v\rho$ is the primary wave velocity in km/s.

We inferred the densities for the other bodies from values for typical rock types (Telford et al., 1990). The geological bodies used include Quaternary volcano-clastic sediments, Pre-rift volcanics, shale and claystone, the Antalo limestone, the Adigrat sandstone, the Proterozoic crystalline basement, and mafic intrusions beneath each caldera complex. We iteratively adjusted the initial model parameters (geometry, depth, and density) by up to 10 % until the calculated gravity values closely matched the observed gravity values. We computed the resulting subsurface models to lessen the root mean square difference (error) between the measured and modeled residual gravity anomalies. Determining what is an acceptable maximum error value is difficult without detailed constraints. Our modeling incorporated regional constraints derived from seismic refraction (basement depth), MT modeling (dense body location), and surface geology. By rigorously applying these constraints, we achieved a strong match between the observed and calculated gravity anomalies. These constraints allowed us to minimize the error between the higher in amplitude and regional anomalies, and not to fit the higher frequency anomalies where we had no constraints. For the latter, we used 0.2 mGal as an error limit, which we based on our previous modeling.

To obtain a 3D configuration of the Corbetti-Shalla caldera complex, we combined the 2D density model along the rift axis (Fig. 9b) and the local topographic map to examine the subsurface magma plumbing system (Fig. 10). We created a topographic map by gridding elevation data to illustrate surface elevation variations across the study area. This topographic map provides the foundation for correlating surface morphology with subsurface structures identified through the various geophysical studies.

4. Results

4.1. Complete Bouguer gravity field

The CBA map (Fig. 4) has gravity maxima (−180 to −164 mGal) over the rift axis caldera complexes (Corbetti and Shalla), eastern rift margin (Wondogenet volcanic zone), the Duguna magmatic zone, and the western rift margin (Wagebeta caldera complex) and gravity minima (−240 to −260 mGal) over the Southeast Plateau.

4.2. Regional and residual gravity field

The regional gravity anomaly map (Fig. 5) has a gravity anomaly trend that decreases toward the NE, reflecting the decrease in crustal thickness between MER and the Southeast Plateau. Within the volcanic complexes, a north-trending maximum that may be due to magmatic intrusions beneath these volcanic complexes.

We identify several short wavelengths anomalies in the residual gravity anomaly field (Fig. 6), which are caused by upper crustal bodies. Of interest to this, the gravity maxima (anomalies 1, 2, and 3) associated

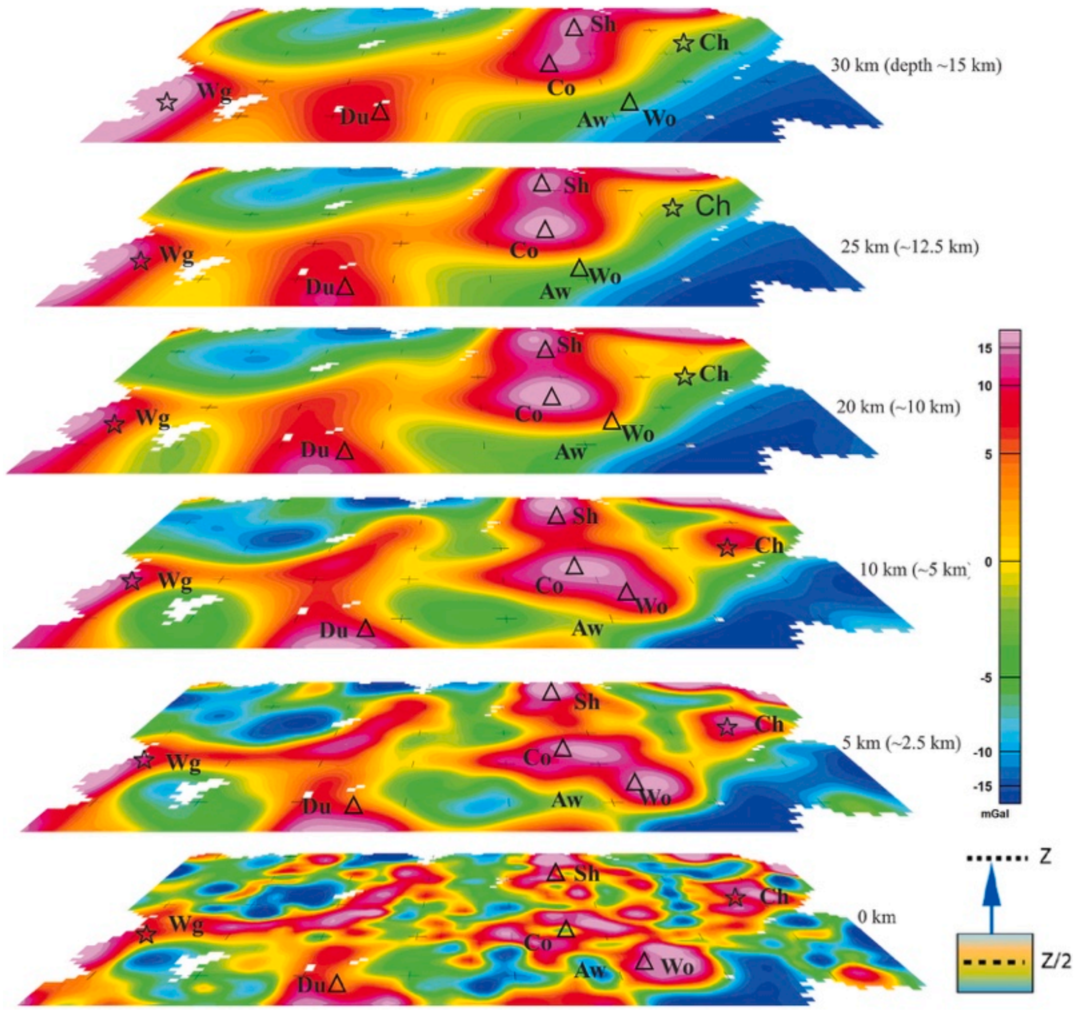

Fig. 7. Upward continuation of the residual gravity anomaly data (Fig. 6) to heights of 5 km, 10 km, 20 km, 25 km, and 30 km to image sources buried at the depths of 2.5 km, 5 km, 10 km, 12.5 km, and 15 km, respectively. The dashed line (Z) represents the continuation height (upward continuation of gravity field data), while (Z/2) corresponds to the approximate depth to the causative bodies, following the methodology of Jacobsen (1987). Abbreviations are the same as in Fig. 4.

with the Quaternary peralkaline silicic caldera complexes (Corbetti and Shalla) and eastern rift margin (Wondo Genet volcanic zone). The thick accumulations of low-density lake sediments and volcanoclastic material in the Awasa, Abiyata, and Langano lakes are responsible for the gravity minima (anomalies 4–6). Anomaly 7 is a north-south trending anomaly that occurs over the Duguna magmatic zone. The off-rift volcanic centers are associated with gravity maxima (anomaly 8). The Southeast Plateau is associated with a gravity minimum (anomaly 9), which is lower in magnitude than seen over the Southwest Plateau.

4.3. Upward continuation and band-pass filtering

The residual gravity field (Fig. 6) was upward continued to heights between 5 and 30 km. Upward continuation provides only an approximate depth estimate, with density anomalies typically situated at depths of half the continuation height or deeper (Jacobsen, 1987), as the exact depth relationship depends on source geometry and lateral extent. We note that this depth relationship is only a rule of thumb; our estimates are approximate because the true depth also depends on the geometry and lateral extent of the density sources. For our continuation heights, this corresponds to depths of 2.5–15 km. Elongated gravity maxima are seen over the caldera complexes (Corbetti and Shalla), the eastern rift margin (Wondo Genet volcanic zone), and Duguna magmatic zone for heights of 0–10 km. Additionally, there are E-W trending gravity maxima over the Wagebeta caldera complex (western rift margin) and the Chike volcanic center (eastern rift shoulder volcano), which is spatially coincident with the transverse structure of the GBVTL (Fig. 1; Lloyd et al., 2018; Corti et al., 2018). On the 10 km continuation map (Fig. 7), we observe that the gravity maximum over the Wondo Genet volcanic zone (eastern rift margin) is no longer seen, indicating that its source is less than 5 km in depth. The 20 km upward continuation map (Fig. 7) suggests that the separate gravity maxima over the Corbetti and Shalla caldera complexes are evident in the residual gravity map (Fig. 6), merge at depth, suggesting the presence of interconnected density sources at depth beneath these caldera complexes, while the anomaly over the Chike sub-volcanic anomaly becomes smaller in amplitude and area. When we continue the upward field to greater heights, it confirms that the Corbetti-Shalla caldera complex exists as one anomaly, while the anomaly over the Duguna magmatic zone retains a high magnitude and appears structurally linked to the Wagebeta caldera complex. The 5 km upward continuation effectively suppresses shallow noise (<5 km), isolating gravity anomalies that correspond to upper-crustal intrusions. This directly images structures such as silicic magma reservoirs and dike swarms, a conclusion strongly supported by MT evidence of a shallow mush zone at approximately 5 km depth beneath the Corbetti caldera complex (Dambly et al., 2024). Conversely, the 10 km continuation filters out both shallow and mid-crustal features to reveal deeper sources. This successfully highlights lower-crustal mafic intrusions, which are consistent with MER-wide observations of such bodies at depths of 10–20 km (Mickus et al., 2007). The 5 km upward continuation

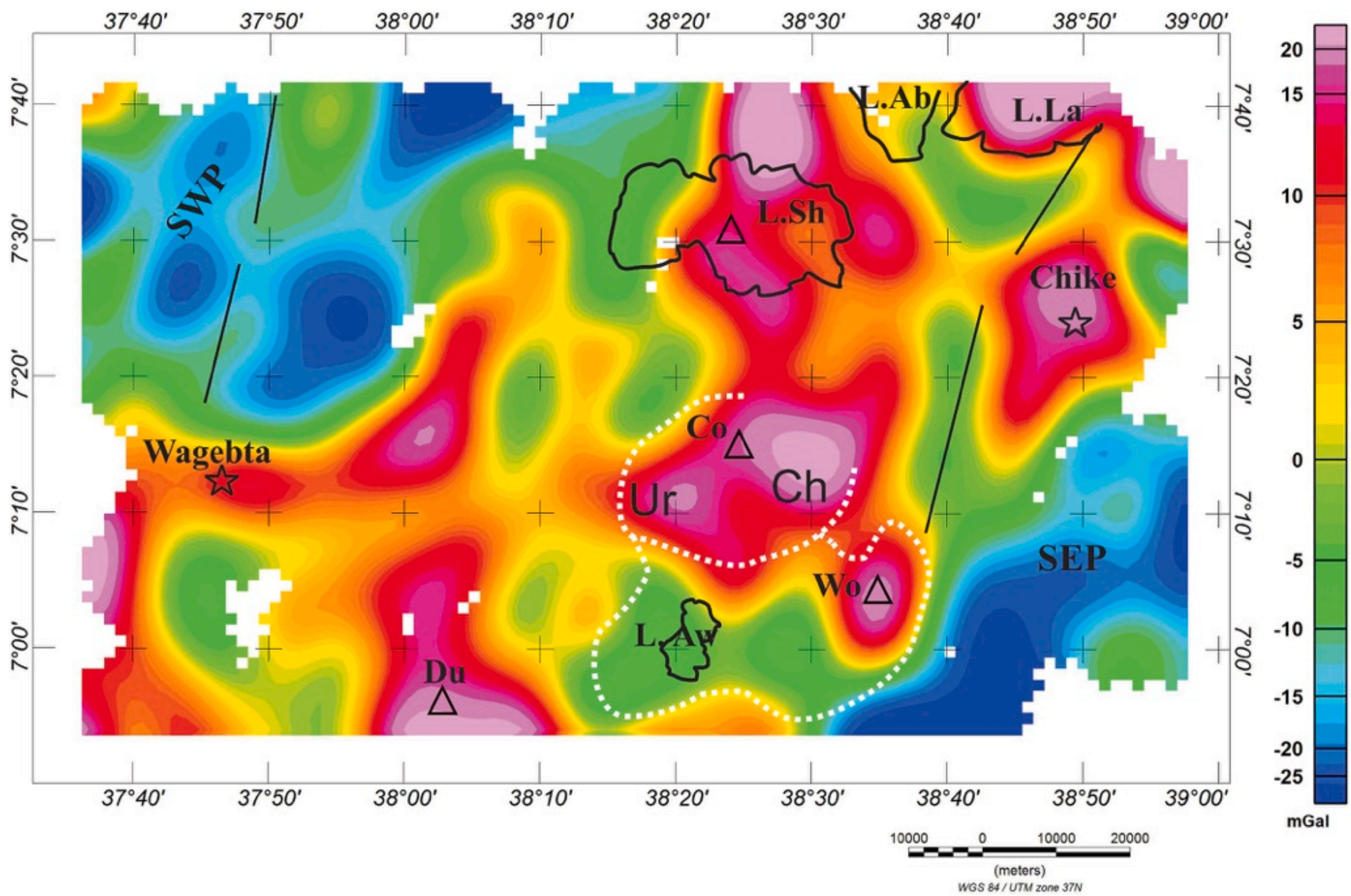

Fig. 8. The band-pass filter gravity anomaly map of the nested ACC and its environs reveals wavelengths between 15 km and 120 km. The black solid lines are rift border faults. Abbreviations and symbols are the same as in Fig. 4.

Table 1
Primary wave velocities (Vp), densities (ρ), and thickness of each subsurface layer used in the gravity modeling (Maguire et al., 2006).

Layer description	Vp (km/s	Initial model ρ (kg/m^3)	Final model ρ (kg/m^3)	Thickness (km)
Quaternary sediments	3	2260	2300	<2
Pre-rift volcanics	5.9	2530	2600	<2
Upper crust (Basement rocks)	6.25	2790	2700	6–20
Mafic Intrusions	6.7	2930	3000	–
Density of Mesozoic sedimentary rocks used for the model (Telford et al., 1990).				
Adigrat sandstone	–	21800	2200	up to 0.4
Variegated shale and claystone	–	24800	2500	up to 0.3
Antalo limestone	–	2410	2420	up to 0.5

effectively suppresses shallow noise (<5 km), isolating gravity anomalies that correspond to upper-crustal intrusions. This directly images structures such as silicic magma reservoirs and dike swarms, a conclusion strongly supported by MT evidence of a shallow mush zone at approximately 5 km depth beneath the Corbetti caldera complex (Dambly et al., 2024). Conversely, the 10 km continuation filters out both shallow and mid-crustal features to reveal deeper sources. This successfully highlights lower-crustal mafic intrusions, which are consistent with MER-wide observations of such bodies at depths of 10–20 km (Mickus et al., 2007).

The band-pass filtered gravity anomaly map was created to support the results and interpretation of the upward continued gravity maps (Fig. 7), and also to identify any density sources between depths of 4–30 km. Roughly, the band-pass filter gravity anomaly map shows similar anomaly patterns as the upward continued gravity anomaly maps continued to heights of 5 and 10 km (Fig. 7). We found that the spatial correlation between the gravity maxima on the band-pass filtered gravity anomaly map correlate spatially with the individual caldera complexes, reinforcing the hypothesis that the density sources associated with these caldera complexes are predominantly localized within the upper crust.

4.4. Gravity modeling and interpretation

Crustal density variations (possible mafic intrusions) and Moho topographic variations are the primary causes of the CBA maxima and minima (Tiberi et al., 2005; Mammo, 2013). Our interpretation of the gravity maxima over the caldera complexes (Fig. 6) is due to upper crustal intrusions, which are consistent with findings from similar volcanic systems (Mickus et al., 2007, 2009). The 20 km upward continued map (Fig. 7) suggests that the individual gravity maxima over the Corbetti and the Shalla caldera complexes have a single gravity maxima, suggesting the presence of interconnected density sources at depth beneath these caldera complexes. In contrast, the gravity maximum associated with the Chike sub-volcanic center diminishes with increasing continuation height, indicating a relatively shallower source depth for this feature. These results reveal a shallow intrusion region, fed by a magma reservoir within the lower crust. This interpretation is supported by a 3D gravity inversion model from Tiberi et al. (2005), which identified mafic intrusions, feeding magma reservoirs beneath Quaternary volcanoes in the MER. The band-pass filtered gravity

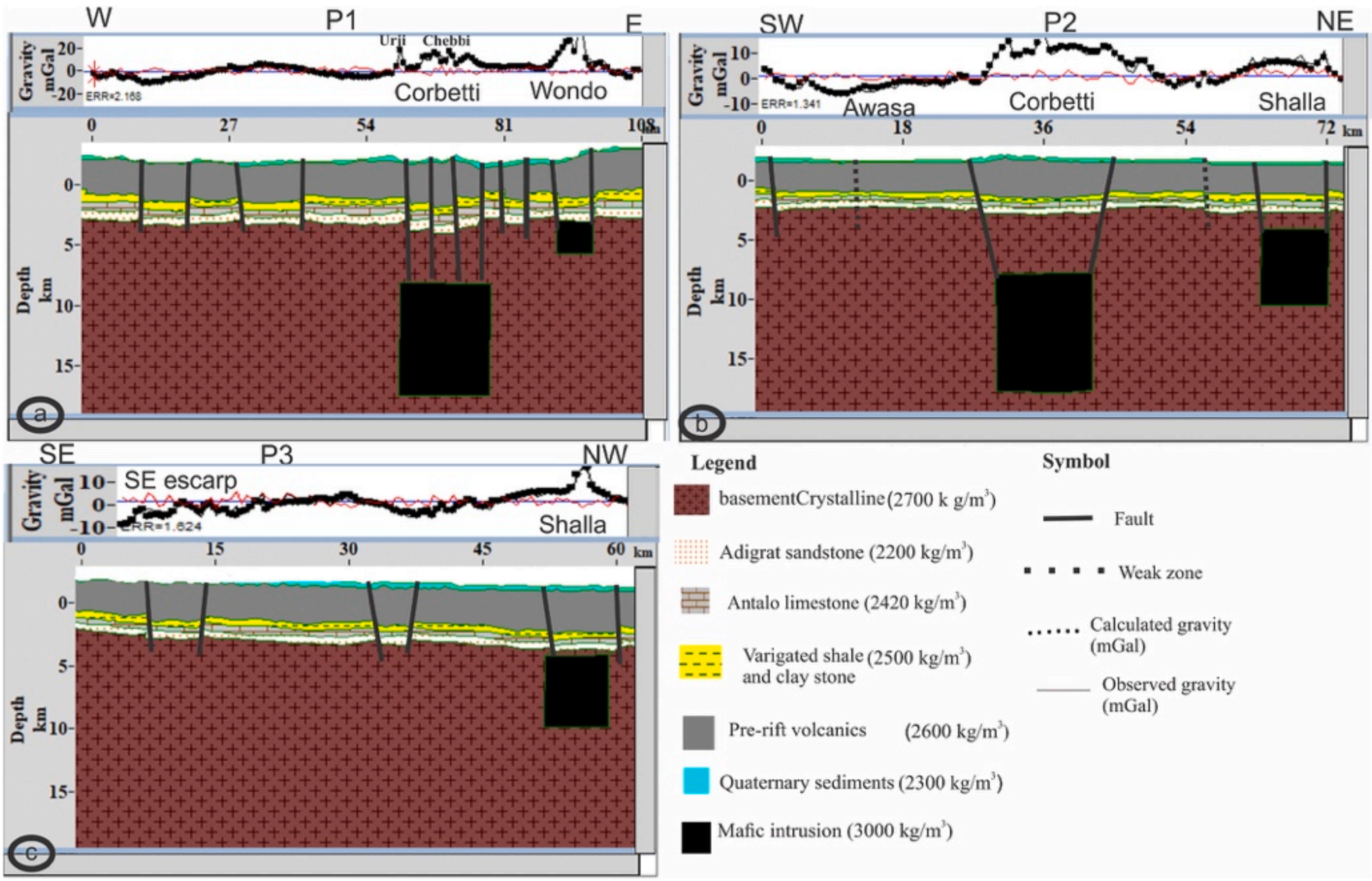

Fig. 9. Two-dimensional (2D) forward gravity models using the residual Bouguer gravity anomaly data (Fig. 6), showing interpreted subsurface density structures along three profiles: (a) P1-cross-sectional profile across the rift floor, (b) P2-longitudinal profile along the rift axis, and (c) P3-oblique profile intersecting the rift axis. Fig. 6 shows the profile location.

anomaly map (Fig. 8) has distinct gravity maxima aligned with the Corbetti-Shalla caldera complexes and the Duguna magmatic zone. We interpret these gravity maxima as evidence for the intrusion of mafic magmas into mid-crustal levels, which possibly recharge the shallow magmatic systems. This interpretation is consistent with geochemical studies modeling the MER magma plumbing systems (Rooney et al., 2011). In addition, gravity maxima over the Wagebeta and Chike volcanoes show that magmatic recharge to the crust is not restricted to the rift axis volcanic centers only, but also to the marginal volcanic zones.

Three gravity models were constructed with one perpendicular to the rift (P1), another parallel to the rift (P2), and one oblique to the rift (P3) (Fig. 6; 9a-c). We used seismic refraction and tomographic models (Keranen et al., 2004; Mackenzie et al., 2005; Maguire et al., 2006) and geological mapping (Fig. 2a and b; Woldegabriel et al., 1990; Abebe et al., 2005) as starting models for our analysis. All three of the models contain the same general bodies from the surface to deeper levels, including Late Quaternary volcanoclastic rocks, including volcanic ash and tuffs, Pre-rift volcanic rocks (Corti, 2009), Mesozoic sedimentary rocks, including variegated shale and claystone, which overlies the Antalo limestone and the Adigrat formation. The Adigrat formation unconformably overlies the Proterozoic basement rocks. The Mesozoic units were included in the models based on scattered outcrops within the study, and their thickness is unknown (Woldegabriel et al., 1990; Abebe et al., 2005).

Model P1 trends from the SW plateau towards the Wondo Genet volcanic zone, crossing the Corbetti caldera complex and the eastern Awasa caldera rim (Figs. 6 and 9a). The goal of developing this model was to characterize the magma plumbing systems (intrusions, shallow magma chambers) of the upper crust, as well as the vertical and horizontal discontinuities, such as buried weak zones and faults beneath the nested ACC. The final model indicates a localized high-density region in the upper crust and may be due to mafic intrusions (Mickus et al., 2007). The Corbetti caldera complex is co-located with a gravity maximum (Fig. 9a), which was modeled to be a mafic intrusion that occurs at a depth of 10 km, at a similar depth determined by Biggs et al. (2011) and Gottsmann et al. (2020). There is an additional intrusion under the Wondo Genet caldera complex, with prominent gravity maxima with narrower wavelengths. The Wonji Fault Belt, caldera ring faults, and border faults (Fig. 2a and b) may be part of the source of small wavelength anomalies along the gravity profile (Fig. 9a). Part of the short wavelength anomalies may be due to faulting within the Precambrian rocks (Woldegabriel et al., 1990).

Model P2 trends along a rift axis beginning from the eastern rift margin (Awasa caldera rim), crossing the center of the Corbetti caldera complex, and then towards the adjacent Shalla caldera complex (Fig. 9b). The upper crustal bodies are similar to those in model P1 (Fig. 9a). Model P2 indicates a relatively shallow mafic intrusion beneath the Shalla caldera complex and a deeper mafic intrusion beneath the Corbetti caldera complex, but there are no deep intrusions beneath the Awasa caldera complex except in the eastern caldera rim (Wondo Genet volcanic zone). We did not model an intrusion beneath Awasa caldera complex because of a negative anomaly on the residual gravity anomaly map (Fig. 6). The caldera ring faults and Werensa ridge (Fig. 2b) offer favorable pathways for the migration of melt from a deep heat source beneath Corbetti caldera complex to the shallow magma chamber beneath Wondo Genet volcanic zone.

Model P3 trends oblique to the rift axis, beginning from the Wondo Genet volcanic zone, crossing the eastern rift margin, and then towards

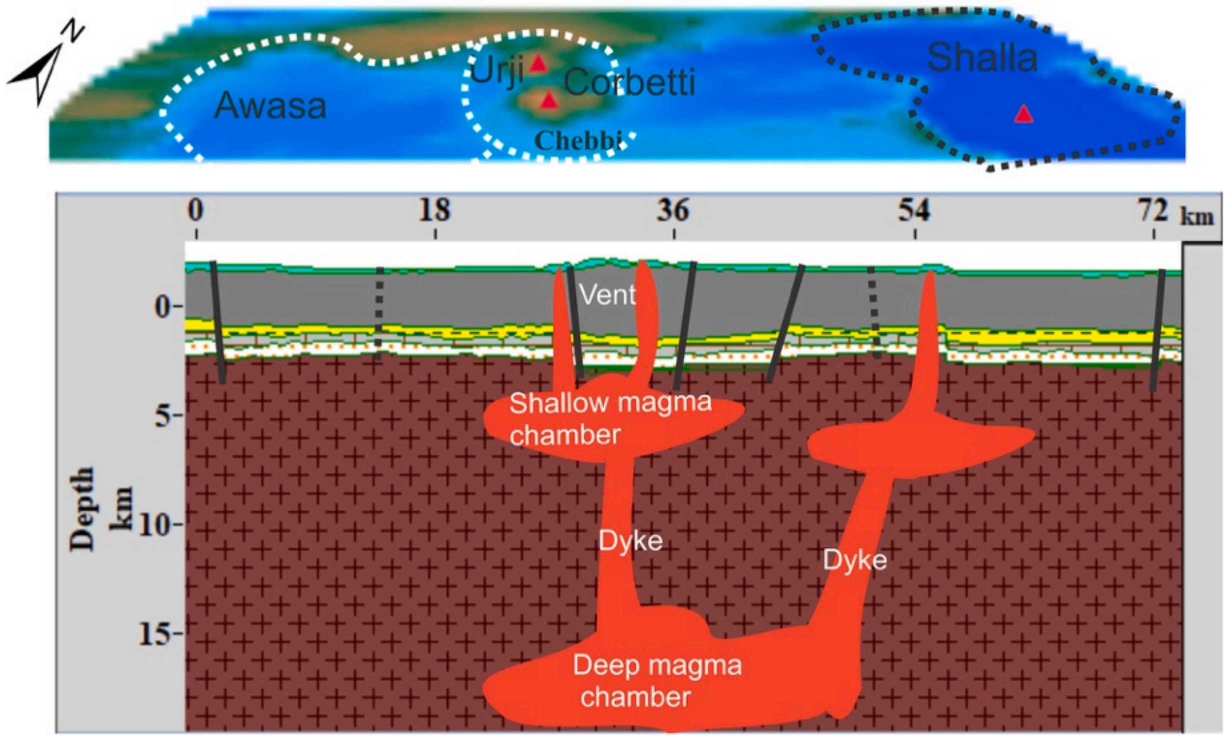

Fig. 10. Schematic diagram of the model P2 (Fig. 9b) showing a potential magma plumbing system beneath the Corbetti–Shalla magmatic zone. The white dotted line represents the nested ACC. The black dotted line represents the Shalla caldera complex. The red triangles are volcanic centers. (For interpretation of the references to color in this figure legend, the reader is referred to the Web version of this article.)

the Shalla caldera complex (Fig. 9c). The densities of the upper crustal bodies are the same as model P1 (Fig. 9a), but the thicknesses and structural layout are different. Model P3 has a mafic intrusion under the Shalla caldera complex, with an upper interface at approximately 7 km. The interaction between Quaternary caldera rim faults and the deeper mafic intrusion under the Shalla caldera complex provides a connection with the shallow magma chambers. Moreover, the short-wavelength maxima beneath the Shalla caldera complex correspond to caldera rim faults.

5. Discussion

The above gravity analysis, combined with the existing geological data (Woldegabriel et al., 1990; Corti et al., 2018), geodetic (Lloyd et al., 2018), and MT and seismic models (Mackenzie et al., 2005; Gíslason et al., 2015; Lavayssière et al., 2019; Gottsmann et al., 2020), provides a better understanding of the subsurface magmatic plumbing systems and their role in rift evolution and the deep magmatic structure beneath the nested calderas.

5.1. Subsurface structure of Awasa-Corbetti caldera complex

Our 2D density models (Fig. 9a–c), supported by upward continued and band-pass filter gravity anomaly maps, reveal dense probably mafic intrusions at various crustal depths at three volcanic regions: 10–20 km beneath Corbetti, 5–7 km beneath Wondo Genet, and 7–12 km beneath Shalla. The spatial distribution of these mafic intrusions is consistent with regional 3D gravity inversion models (Tiberi et al., 2005) that interpreted mafic intrusions fed magma reservoirs in the rift-controlled Quaternary volcanoes within the MER. In addition, the occurrence of surface thermal springs found within the Shalla, Corbetti, and Wondo Genet volcanic zones suggests the presence of geothermal resources and possibly magma within the crust (Wassihun et al., 2025).

The modeled intrusion depths (10–20 km) beneath Corbetti show consistency with intrusion depths to regional seismic imaging (Keranen et al., 2004; Daly et al., 2008) and MT models (Whaler and Hautot, 2006). These later studies proposed mafic intrusions beneath the magmatic segments within the CMER and NMER at depths between 12 and 25 km.

At the Corbetti caldera complex, 3D MT models identified two electrically conductive zones: a shallow region <2 km and the deeper feature >10 km (Gíslason et al., 2015). These conductivity anomalies coincide with the upper and lower depth bounds of the gravity-derived dense (mafic) intrusions (Fig. 9a–c). Our model suggests that these zones in the upper 10 km represent the currently deforming magma reservoir, with active hydrothermal circulation above it. The presence of magma within these dense mafic intrusions indicates that the Corbetti magmatic system has remained active sufficiently long to generate substantial volumes of mafic intrusions and prolonged magmatic activity at the Corbetti caldera complex that enabled the accumulation of substantial intrusive volumes. Critically, the MT derived high electrical conductivities suggest that the intrusions retain 6–16 % basaltic melt by volume in the lower crust, supporting the existence of a transcrustal magma system. Magma melt from this system migrates upward, accumulating as a crystal-rich mush within shallow crustal reservoirs beneath the caldera complex (Dambly et al., 2024). A geodetic and gravity study (Gottsmann et al., 2020) interpreted the occurrence of a mafic intrusion with a molten crystal mush zone beneath the Corbetti caldera complex at an approximate depth of 7 km (Fig. 3c). We interpret this intrusion as a promising heat source for a prospective geothermal site at the Corbetti Caldera complex.

The subsurface magmatic structure consists of interconnecting magma conduits and shallow magma reservoirs that hold magma as it grows into crystal mush and is eventually supplied from a zone of partial melting in the asthenosphere (Magee et al., 2018). We used MT models to support the interpretation of a deep connected magma chamber (Figs. 10 and 11). Thus, our conceptual model is supported by the upward continued gravity map (Fig. 7), which indicates that the Corbetti

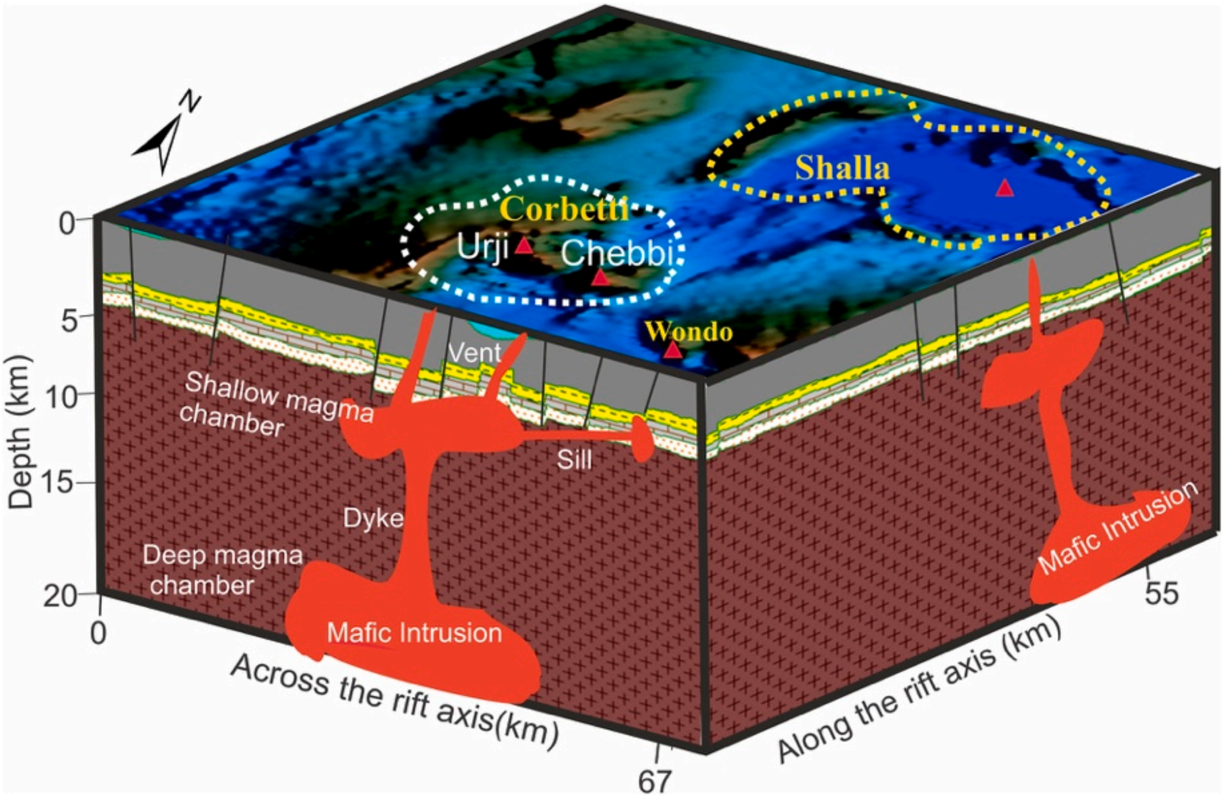

Fig. 11. The 3D magmatic structures of the upper crust for the nested Awasa–Corbetti caldera and its environs. The red stars are the volcanic centers, the white dotted lines represent the Corbetti caldera complex, and the yellow dotted line represents the Shalla caldera complex. The red triangles are volcanic centers. (For interpretation of the references to color in this figure legend, the reader is referred to the Web version of this article.)

and Shalla caldera complexes both have mafic intrusions at approximately the same depth, but the intrusions become discrete at an approximate depth of 10 km. Our model suggests that the two caldera complexes are fed by a deep magma source and that there are additional smaller, high-density bodies formed by magmatic processes located at shallower depths beneath each caldera complex. This interpretation of a vertically stratified magmatic system agrees with the geochemical analysis of Corti et al. (2018), which found Hf and Zr enrichment beneath the Corbetti caldera complex. This enrichment indicates crustal modification from partial melting and suggests magma resides at shallow crustal depths. These findings are consistent with our geophysical models (Figs. 10 and 11). This configuration is common within the CMER and NMER as similar models have been interpreted at the Bora, Bericha, and Tullu Moye Caldera complexes, north of the Corbetti caldera complex (Nigussie et al., 2023b), and indicates that there are multiple volcanoes within a magmatic segment being fed from a single deeper reservoir in the lower crust. Our interpretation is consistent with and supported by seismic refraction models, which show widespread elevated P-wave velocity regions in the lower crust (Mackenzie et al., 2005; Maguire et al., 2006). This observation agrees with geochemical (Hutchison et al., 2016a) and isotopic studies (Hutchison et al., 2018), where there are two shallow magma reservoirs beneath the magmatic segments.

5.2. *Off-rift volcanic zones*

A close examination of the residual, upward continued, and band-pass filtered gravity anomaly maps (Figs. 6–8) indicated prominent gravity maxima along both the rift axis and off-rift zones. We interpret these gravity maxima as evidence of magmatic recharge into the upper crust. This interpretation is consistent with models of magma-assisted rifting in continental rift zones (Keir et al., 2009). Furthermore, we observe that the gravity maxima beneath the rift floor spatially correlates with the Duguna, Corbetti, and Shalla volcanic centers. This spatial correlation suggests to us that there is sustained magma storage and crustal melt accumulation beneath the rift axis, a concept also discussed by Rooney et al. (2011) and Hutchison et al. (2016b). Notably, we also identified gravity maxima associated with off-rift volcanoes such as Wagebeta and Chike, and the eastern Awasa caldera complex rim (Wondo Genet volcanic zone). This leads us to conclude that magmatic replenishment is not limited to the axial rift but also extends to the off-rift regions, a process likely facilitated by pre-existing crustal structures. Previous works support this conclusion as Keir et al. (2009) stress that magma-induced seismicity is distributed both within and away from the rift axis. Similarly, Ebinger and Casey (2001) showed that magmatism could extend beyond the rift axis due to decompression melting and shifts in tectonic stress, which supports our assertion of off-rift magmatic replenishment.

5.3. *The role of the GBVTL as a magmatic pathway*

The GBVTL is a pre-existing structural lineament that traverses the rift from the western flank to the nested ACC, evidenced from surface structural mapping (Fig. 1; Korme et al., 2004; Corti, 2009). Gravity maxima on the residual (Fig. 6), upward-continued (Fig. 7), and band-pass filtered (Fig. 8) anomaly maps occur over the GBVTL, suggesting that this structure is underlain by high-density material, likely mafic intrusions or accumulated crystallized magma at depth. This correlation implies that the GBVTL serves as a preferential magma pathway, facilitating melt migration from deeper crustal or mantle sources toward the surface.

6. Conclusions

The integration of gravity data with existing geological and geophysical data, and models from the ACC region has provided insights into the subsurface magmatic and tectonic structures and the role of magma replenishment in shaping the evolution of the CMER. Gravity anomaly maps, including complete Bouguer, residual, upward continued, and band-pass filtered, indicate that gravity maxima occur Corbetti and Shalla caldera complexes, and Wondo Genet volcanic zones. The 2D gravity models constrained by seismic and MT models, and geological maps revealed the presence of mafic intrusions extending to the estimated depth range of 10–20 km beneath Corbetti caldera complex, 7–12 km beneath Shalla caldera complex, and 5–7 km beneath Wondo Genet volcanic zone. These models, geological and geodetic data, and seismic and magnetotelluric models were incorporated into a 3D conceptual model that is interpreted to show that deep mafic intrusions and dikes feed a shallow magma system beneath the Corbetti and Shalla caldera complexes correspondingly. Our 2D models reveal the absence of deep-seated mafic intrusions beneath the Awasa caldera complex, which suggests that the shallow mafic intrusions at the Wondo Genet volcanic zone are probably fed by deep melt sources from the Corbetti caldera complex as a sill body. Additionally, off-rift volcanic zones (Wagebeta and Chike volcanoes) inferred from upward continued and band-pass gravity anomaly maps, supported by geochemical data, suggest that magmatic recharge by dike injection is also taking place near the rift margins. These findings contribute to the growing body of knowledge that volcanic centers within the CMER host interconnected magmatic systems, which drive crustal modification through dike emplacement. Dike-dominated crustal accretion and modification not just passive stretching drives rift evolution in the middle and later stages of rift evolution. Our results indicate that the rift evolution is not confined to the axial rift but also involves magmatic addition just outside the boundaries of the rift.

CRediT authorship contribution statement

Simeneh Wassihun: Writing – original draft, Project administration, Formal analysis, Conceptualization. **Abera Alemu:** Supervision. **Wubamlak Nigussie:** Writing – original draft, Conceptualization. **Kevin Mickus:** Writing – original draft, Conceptualization. **Derek Keir:** Writing – review & editing, Writing – original draft. **Shimels Wendwesen:** Writing – review & editing, Writing – original draft. **Habtamu Wuletawu:** Writing – review & editing, Writing – original draft.

Data availability statement

The corresponding author provided the gravity data for this research, and they can be obtained from him.

Declaration of competing interest

Corresponding author, on behalf of all the authors of the submission, disclose any financial and personal relationships with other people or organizations that could inappropriately influence or bias their work. All the authors declare no financial or scientific conflicts of interest concerning the paper's results.

Acknowledgments

The authors would like to express their sincere gratitude to the National Geospatial and Imaging Agency of the USA for providing the terrestrial gravity dataset. The authors would like to thank the reviewers and Barbara Tewksbury for insightful comments and suggestions that greatly improved the paper.

References

Abebe, T., Manetti, P., Bonini, M., Corti, G., Innocenti, F., Mazzarini, F., Pecskay, Z., 2005. Geological map (scale 1: 200,000) of the northern Main Ethiopian Rift and its implication for the volcano-tectonic evolution of the rift. Geol. Soc. Am. Bull. 821, 51–97.

Abera, A., 2020. Geophysics: Principles, Practice and Application of Geophysical Methods to Resource Exploration and Geohazard Studies. Aster Nega Publishing Enterprises.

Acocella, V., Korme, T., Salvini, F., Funiciello, R., 2002. Elliptic calderas in the Ethiopian Rift: control of pre-existing structures. J. Volcanol. Geoth. Res. 119 (1–4), 189–203.

Benti, N.E., Woldegiyorgis, T.A., Geffe, C.A., Gurmesa, G.S., Chaka, M.D., Mekonnen, Y. S., 2023. Overview of geothermal resources utilization in Ethiopia: potentials, opportunities, and challenges. Sci. Afr. 19, e01562.

Biggs, J., Anthony, E.Y., Ebinger, C.J., 2009. Multiple inflation and deflation events at Kenyan volcanoes, East African Rift. Geology 37 (11), 979–982.

Biggs, J., Bastow, I.D., Keir, D., Lewi, E., 2011. Pulses of deformation reveal frequently recurring shallow magmatic activity beneath the Main Ethiopian Rift. G-cubed 12 (9). https://doi.org/10.1029/2011GC003662.

Boccaletti, M., Bonini, M., Mazzuoli, R., Abebe, B., Piccardi, L., Tortorici, L., 1998. Quaternary oblique extensional tectonics in the Ethiopian Rift (Horn of Africa). Tectonophysics 287 (1–4), 97–116.

Bonini, M., Corti, G., Innocenti, F., Manetti, P., Mazzarini, F., Abebe, T., Pecskay, Z., 2005. Evolution of the Main Ethiopian Rift in the frame of Afar and Kenya rifts propagation. Tectonics 24 (1), 1–21. https://doi.org/10.1029/2004TC001680.

Buck, W.R., 2006. The Role of Magma in the Development of the Afro-Arabian Rift System.

Casey, M., Ebinger, C., Keir, D., Gloaguen, R., Mohamed, F., 2006. Strain accommodation in transitional rifts: extension by magma intrusion and faulting in Ethiopian rift magmatic segments. Geol. Soci. 259 (1), 143–163. http://sp.lyellcollection.org/.

Chambers, E.L., Harmon, N., Keir, D., Rychert, C.A., 2019. Using ambient noise to image the northern East African Rift. G-cubed 20, 2091–2109.

Chambers, E.L., Harmon, N., Rychert, C.A., Keir, D., 2021. Variations in melt emplacement beneath the northern East African Rift from radial anisotropy. Earth Planet Sci. Lett. 573, 117150.

Chambers, E.L., Harmon, N., Rychert, C.A., Gallacher, R.J., Keir, D., 2022. Imaging the seismic velocity structure of the crust and upper mantle in the northern East African Rift using Rayleigh wave tomography. Geophys. J. Int. 230 (3), 2036–2055.

Christensen, N., Mooney, W., 1995. Seismic velocity structure and composition of the continental crust: a global view. J. Geophys. Res. 100, 9761–9788.

Colby, D.J., Pyle, D.M., Fontijn, K., Mather, T.A., Melaku, A.A., Mengesha, M.A., Yirgu, G., 2022. Stratigraphy and eruptive history of Corbetti Caldera in the Main Ethiopian Rift. J. Volcanol. Geoth. Res. 428, 107580.

Corti, G., 2009. Continental rift evolution: from rift initiation to incipient break-up in the Main Ethiopian rift, East Africa. Earth Sci. Rev. 96 (1–2), 1–53.

Corti, G., Sani, F., Agostini, S., Philippon, M., Sokoutis, D., Willingshofer, E., 2018. Off-axis volcano-tectonic activity during continental rifting: insights from the transversal Goba-Bonga lineament, Main Ethiopian Rift (East Africa). Tectonophysics 728, 75–91.

Daly, E., Keir, D., Ebinger, C.J., Stuart, G.W., Bastow, I.D., Ayele, A., 2008. Crustal tomographic imaging of a transitional continental rift: the Ethiopian rift. Geophys. J. Int. 172 (3), 1033–1048. https://doi.org/10.1111/j.1365-246X.2007.03682.x.

Dambly, M.L., Samrock, F., Grayver, A., Eysteinsson, H., Saar, M.O., 2024. Geophysical imaging of the active magmatic intrusion and geothermal reservoir formation beneath the Corbetti prospect, Main Ethiopian Rift. Geophys. J. Int. ggad493.

Di Paola, G.M., 1971. Geology of the Corbetti caldera area (Main Ethiopian rift Valley). Bull. Volcanol. 35 (2), 497–506.

Di Paola, G.M., 1972. The Ethiopian Rift Valley (Between 7 ° off and 8 ° 40' lat. North). Bull. Volcanol. 36 (4), 517–560.

Ebinger, C.J., Casey, M., 2001. Continental breakup in magmatic provinces: an Ethiopian example. Geology 29 (6), 527–530.

EIGS (Ethiopian Institute of Geological Survey), 2012. Geology Geochemistry and Gravity Survey of the Hossana Area. Unpublished technical report. Memoir no. 36.

Gíslason, G., Eysteinsson, H., Björnsson, G., Harðardóttir, V., 2015. Results of surface exploration in the Corbetti Geothermal Area, Ethiopia. In: World Geothermal Congress, pp. 19–25. Melbourne, Australia.

Gottsmann, J., Biggs, J., Lloyd, R., Biranhu, Y., Lewi, E., 2020. Ductility and compressibility accommodate high magma flux beneath a silicic continental rift caldera: insights from Corbetti caldera (Ethiopia). G-cubed 21, e2020GC008952.

Hammond, J.O., Kendall, J.M., Stuart, G.W., Keir, D., Ebinger, C., Ayele, A., Belachew, M., 2011. The nature of the crust beneath the Afar triple junction: evidence from receiver functions. G-cubed 12 (12).

Hayward, N.J., Ebinger, C.J., 1996. Variations in the along-axis segmentation of the Afar Rift system. Tectonics 15 (2), 244–257. https://doi.org/10.1029/95TC02292.

Hinze, W.J., von Frese, R.R., Saad, A.H., 2013. Gravity and Magnetic Exploration Principles, Practices, and Applications. Cambridge University Press.

Hunt, J.A., Pyle, D.M., Mather, T.A., 2019. The geomorphology, structure, and lava flow dynamics of peralkaline rift volcanoes for high-resolution digital elevation models. G-cubed 20 (3), 1508–1533.

Hutchison, W., Biggs, J., Mather, T.A., Pyle, D.M., Lewi, E., Yirgu, G., Caliro, S., Chiodini, G., Clor, L.E., Fischer, T.P., 2016a. Causes of unrest at silicic calderas in the East African Rift: new constraints from InSAR and soil-gas chemistry at Aluto volcano, Ethiopia. G-cubed 17 (8), 3008–3030.

Hutchison, W., Fusillo, R., Pyle, D., Mather, T., Blundy, J., Biggs, J., Yirgul, G., Cohen, B., Brooker, R., Bardod, D., Calvert, A., 2016b. A pulse of mid-Pleistocene volcanism in Ethiopia at the dawn of modern humans. Nat. Commun. 7, 13192.

Hutchison, W., Mather, T.A., Pyle, D.M., Boyce, A.J., Gleeson, M.L., Yirgu, G., Finch, A. A., 2018. The evolution of magma during continental rifting: new constraints from the isotopic and trace element signatures of silicic magmas from Ethiopian volcanoes. Earth Planet Sci. Lett. 489, 203–218.
Jacobsen, B.H., 1987. A case for upward continuation as a standard separation filter for potential-field maps. Geophysics 52 (8), 1138–1148.
Keranen, K., Klemperer, S.L., Gloaguen, R., Asfaw, L., Ayele, A., Ebinger, C., Furman, T., Harder, S., Keller, G.R., Mackenzie, G.D., Maguire, P.K.H., Stuart, G.W., 2004. Three-dimensional seismic imaging of a protoridge axis in the Main Ethiopian rift. Geology 32 (11), 949–952.
Keir, D., Hamling, I.J., Ayele, A., Calais, E., Ebinger, C., Wright, T.J., Bennati, L., 2009. Evidence for focused magmatic accretion at segment centers from lateral dike injections captured beneath the Red Sea rift in Afar. Geology 37 (1), 59–62.
Kibret, B.A., Ayele, A., Keir, D., 2022a. Modeling S-wave velocity structure beneath the central main Ethiopian rift using receiver functions. Front. Earth Sci. 10, 773783.
Kibret, B.A., Ayele, A., Keir, D., 2022b. Crustal structure of the Ethiopian northwestern Plateau and central Afar from receiver function analysis. Front. Earth Sci. 11. https://doi.org/10.3389/feart.2023.1170907.
Korme, T., Acocella, V., Abebe, B., 2004. The role of pre-existing structures in the origin, propagation and architecture of faults in the Main Ethiopian Rift. Gondwana Res. 7 (2), 467–479.
Kurz, T., Gloaguen, R., Ebinger, C., Casey, M., Abebe, B., 2007. Deformation distribution and type in the Main Ethiopian Rift (MER): a remote sensing study. J. Afr. Earth Sci. 48 (2–3), 100–114.
Lavayssière, A., Greenfield, T., Keir, D., Ayele, A., Kendall, J.M., 2019. Local seismicity near the actively deforming Corbetti volcano in the Main Ethiopian Rift. J. Volcanol. Geoth. Res. 381, 227–237.
Liu, Y.A., Murphy, M.A., van Wijk, J., Koning, D.J., Smith, T., Andrea, R.A., 2019. Progressive opening of the northern Rio Grande rift based on fault structure and kinematics of the Tusas-Abiquiu segment in north-central New Mexico, US. Tectonophysics 753, 15–35.
Lloyd, R., Biggs, J., Wilks, M., Nowacki, A., Kendall, J.M., Ayele, A., Lewi, E., Eysteinsson, H., 2018. Evidence for cross rift structural controls on deformation and seismicity at a continental rift caldera. Earth Planet. Lett. 487, 190–200.
Luthfian, A., Eccles, J.D., Miller, C.A., 2023. Gravity and magnetic models at Rangitoto Volcano, Auckland Volcanic Field, New Zealand: implications for basement control on magma ascent. J. Volcanol. Geoth. Res. 439, 107824.
Mackenzie, G.D., Thybo, H., Maguire, P.K.H., 2005. Crustal velocity structure across the Main Ethiopian Rift: results from two-dimensional wide-angle seismic modeling. Geophys. J. Int. 162 (3), 994–1006. https://doi.org/10.1111/j.1365-246X.2005.02710.x.
Maestrelli, D., Corti, G., Bonini, M., Montanari, D., Sani, F., 2021. Caldera collapse and tectonics along the Main Ethiopian Rift: reviewing possible relationships. C. R. Geosci. 353 (S2), 1–19. https://doi.org/10.5802/CRGEOS.63.
Magee, C., Stevenson, C.T., Ebmeier, S.K., Keir, D., Hammond, J.O., Gottsmann, J.H., Jackson, M.D., 2018. Magma plumbing systems: a geophysical perspective. J. Petrol. 59 (6), 1217–1251.
Maguire, P.K.H., Keller, G.R., Klemperer, S.L., Mackenzie, G.D., Keranen, K., Harder, S., O'reilly, B., Thybo, H., Asfaw, L., Khan, M.A., Amha, M., 2006. Crustal structure of the northern Main Ethiopian Rift from the EAGLE controlled-source survey; a snapshot of incipient lithospheric break-up. Geological Soc. London Special Publ. 259 (1), 337–340.
Mahatsente, R., Jentzsch, G., Jahr, T., 1999. Crustal structure of the Main Ethiopian Rift from gravity data: 3-dimensional modeling. Tectonophysics 313 (4), 363–382.
Mammo, T., 2013. Crustal structure of the flood basalt province of Ethiopia from constrained 3-D Gravity Inversion. Pure Appl. Geophys. 170 (12), 2185–2206.
Mickus, K., Kennedy, D., Aiken, C., 1992. Regional-residual gravity anomaly separation using the minimum curvature method. Geophysics 56, 279–283.
Mickus, K., Tadesse, K., Keller, G.R., Oluma, B., 2007. Gravity analysis of the main Ethiopian rift. J. Afr. Earth Sci. 48, 59–69.
Mickus, K., Ketsela, K., Keller, G., Oluma, B., 2009. Three-dimensional gravity modeling of the magmatic segments within the Main Ethiopian Rift. Tanzanian J. Earth Sci. 1, 96–106.
Nigussie, W., Alemu, A., Mickus, K., Muluneh, A.A., 2022. Structure of the upper crust at the axis segmentation stage of rift evolution as revealed by gravity data: case study of the Gedemsa magmatic segment, Main Ethiopian Rift. J. Afr. Earth Sci. 190, 104523.
Nigussie, W., Alemu, A., Muluneh, A.A., Mickus, K., Muhabaw, Y., 2023a. Formation of magmatic segments within the Aluto-Gedemsa area, Main Ethiopian Rift. Italian J. Geosci. 142 (1), 28–41.
Nigussie, W., Alemu, A., Mickus, K., Keir, D., Demissie, Z.S., Muhabaw, Y., Yehualaw, E., 2023b. Subsurface structural control of geothermal resources in a magmatic rift: gravity and magnetic study of the Tulu Moye geothermal prospect, Main Ethiopian Rift. Front. Earth Sci. 11, 1181533.
Peccerillo, A., Barberio, M.R., Yirgu, G., Ayalew, D., Barbieri, M., Wu, T.W., 2003. Relationships between mafic and peralkaline silicic magmatism in continental rift settings: a petrological, geochemical and isotopic study of the Gedemsa volcano, Central Ethiopian rift. J. Petrol. 44, 2003–2031.
Rapprich, V., Žáček, V., Verner, K., Erban, V., Goslar, T., Bekele, Y., Hejtmánková, P., 2016. Wendo Koshe Pumice: the latest Holocene silicic explosive eruption product of the Corbetti volcanic system (southern Ethiopia). J. Volcanol. Geoth. Res. 310, 159–171.
Rooney, T.O., Bastow, I.D., Keir, D., 2011. Insights into extensional processes during magma assisted rifting: evidence from aligned scoria cones. J. Volcanol. Geoth. Res. 201, 83–96.
Saltus, R.W., Blakely, R.J., 2011. Unique geologic insights from non-unique gravity and magnetic interpretation. GSA Today (Geol. Soc. Am.) 21 (12), 4–11.
Siegburg, M., Bull, J.M., Nixon, C.W., Keir, D., Gernon, T.M., Corti, G., Ayele, A., 2020. Quantitative constraints on faulting and fault slip rates in the northern Main Ethiopian Rift. Tectonics 39 (8), e2019TC006046.
Stuart, G.W., Bastow, I.D., Ebinger, C.J., 2005. Crustal Structure of the northern Main Ethiopian Rift from receiver function studies. TAfar Volcanic Province within East Afr. Rift System 259, 253–267. Geological Society of London Special Publication.
Telford, W.S., Geldart, L.P., Sheriff, R.E., 1990. Applied Geophysics, second ed. Cambridge University Press.
Tiberi, C., Ebinger, C., Ballu, V., Stuart, G., Oluma, B., 2005. Inverse models of gravity data from the Red Sea Aden-East African rifts triple junction zone. Geophys. J. Int. 163 (2), 775–787. https://doi.org/10.1111/j.1365-246X.2005.02736.
Wassihun, S., Alemu, A., Nigussie, W., Mickus, K., Workie, M.D., Wuletawu, H., Yehualaw, E., 2025. Application of surface and subsurface anomaly linkage in geothermal resource evaluation: a case study of the Corbetti geothermal prospect, main Ethiopian rift. Geothermics 125, 103191.
Wendwesen, S., Alemu, A., Nigussie, W., Mickus, K., Wassihun, S., Wuletawu, H., Muhabaw, Y., 2025. Tectonic and magmatic segmentation interlinkage in the central main Ethiopian rift. Tectonophysics, 230725.
Whaler, K.A., Hautot, S., 2006. The electrical resistivity structure of the crust beneath the northern Main Ethiopian Rift. Geological Soc. London Special Publ. 259 (1), 293–305.
Woldegabriel, G., Aronson, J., Walter, R., 1990. Geology, geochronology, and rift basin development in the central sector of the Main Ethiopia Rift. Geol. Soc. Am. Bull. 102, 439–458.
Wolfenden, E., Ebinger, C., Yirgu, G., Deino, A., Ayalew, D., 2004. Evolution of the northern Main Ethiopian rift: birth of a triple junction. Earth Planet Sci. Lett. 224, 213–228.
Wuletawu, H., Alemu, A., Nigussie, W., Mickus, K., Keir, D., Wendwesen, S., Wassihun, S., 2024. The subsurface anatomy of a mid-upper crustal magmatic intrusion zone beneath the Boku volcanic complex, Main Ethiopian Rift inferred from gravity data. J. Volcanol. Geoth. Res. 452, 108133.
Wuletawu, H., Alemu, A., Nigussie, W., Mickus, K., Keir, D., Wassihun, S., Wendwesen, S., 2025. The link between geothermal resources and subsurface geological structures in the magma-rich Ethiopian rift: a case study of the Boku geothermal prospect. J. Volcanol. Geoth. Res., 108333